REPORT DOCUMENTATION PAGE

AFRL-SR-AR-TR-04-

0050

1. REPORT DATE (DD-MM-YYYY)	2. REPORT TYPE	3. DATES COVERED (From - To)
29-12-2003	Final	01-04-1997 - 30-09-2000

4. TITLE AND SUBTITLE
Superconducting and Magnetically Ordered Systems

5a. CONTRACT NUMBER

5b. GRANT NUMBER
F49620-97-1-0297

5c. PROGRAM ELEMENT NUMBER

6. AUTHOR(S)
C.E. Stronach and D.R. Noakes

5d. PROJECT NUMBER

5e. TASK NUMBER

5f. WORK UNIT NUMBER

7. PERFORMING ORGANIZATION NAME(S) AND ADDRESS(ES)

Department of Physics
Box 9325
Virginia State University
Petersburg, VA 23806

8. PERFORMING ORGANIZATION REPORT NUMBER

4.

9. SPONSORING / MONITORING AGENCY NAME(S) AND ADDRESS(ES)
Air Force Office of
Scientific Research
C/o Dr. Harold Weinstock
4015 Wilson Blvd., Rm. 713
Arlington, VA 22203-1954

10. SPONSOR/MONITOR'S ACRONYM(S)
AFOSR

11. SPONSOR/MONITOR'S REPORT NUMBER(S)

12. DISTRIBUTION / AVAILABILITY STATEMENT
Distribution Statement A:

APPROVED FOR PUBLIC RELEASE,
DISTRIBUTION UNLIMITED

13. SUPPLEMENTARY NOTES

14. ABSTRACT

This Report covers the period of grant F49620-97-1-0297, from April 1, 1997 to September 30, 2000. The major research findings include (a) determination of the exotic magnetic and superconducting behavior of Sr_2YRuO_6, (b) discovery of coexistence of ferromagnetism and superconductivity in $RuSr_2GdCu_2O_8$, (c) determination of the correct expression for the strong-collision Lorentzian in fast fluctuations or high fields, (d) measurement of correlation lengths in the disordered magnetic alloys $CeNi_{1-x}Cu_xSn$, (e) a study of the vortex-core structure of superconducting YBCO done with muon spin rotation, (f) preparation for publication of *μSR studies of rare earth and actinide magnetism* in the *Handbook on the Physics and Chemistry of Rare Earths*, (g) a study of spin dynamics and freezing in magnetic rare-earth quasicrystals, and (h) a study of non-Fermi-liquid metallic Ce_7Ni_3.

15. SUBJECT TERMS

16. SECURITY CLASSIFICATION OF:			17. LIMITATION OF ABSTRACT	18. NUMBER OF PAGES	19a. NAME OF RESPONSIBLE PERSON
a. REPORT	b. ABSTRACT	c. THIS PAGE		13 plus 31 app.	Carey E. Stronach
					19b. TELEPHONE NUMBER (include area code) 804-524-5915

Final Report

Superconducting and Magnetically Ordered Systems Research Program

Physics Department
Virginia State University
Petersburg, VA 23806

for the period

April 1, 1997 - September 30, 2000

supported by the

Air Force Office of Scientific Research
Grant No. F49620-97-1-0297

Carey E. Stronach, Ph.D.
Project Director

David R. Noakes, Ph.D.
Associate Director

Summary

During the three years that the Superconducting and Magnetically Ordered Systems Research Program at Virginia State University was supported by the Air Force Office of Scientific Research, considerable progress was made in these areas of study, and the groundwork was laid for further research that has been extremely fruitful.

During these three years, members of the group, primarily Dr. David R. Noakes, performed a number of studies on magnetically-ordered systems. These include f-electron magnetic systems, Kondo-lattice CeTSn (T = transition metal), strong-collision dynamics in PrP_x, rare-earth - transition-metal intermetallics, non-Fermi liquid Ce_7Ni_3, range-correlated magnetic-moment variation, rare-earth quasicrystals, neutron scattering studies of chromium alloys, and magnetic frustration and competing exchange. This report will focus on range-correlated magnetic-moment variation, rare-earth quasicrystals, and magnetic frustration.

During this same period, members of the group, primarily Dr. Carey E. Stronach, performed a number of muon-spin-rotation experiments on high-temperature superconductors at the TRIUMF cyclotron laboratory. A major focus of this work was the interplay between superconductivity and magnetic ordering in these ceramic materials. These phenomena are elaborated upon in this report.

This report also contains a listing of the 26 papers published by the VSU group during this three-year period. Finally, this program provided excellent research experiences for participating students, most of whom are members of minority groups.

High-Temperature Superconductivity

An important discovery in this area was the result of a study of the ceramic compound $Sr_2YRu_{1-u}Cu_uO_6$, done at TRIUMF using the muon spin rotation (μSR) technique. Two signals were observed below the Curie and Néel temperatures (both ~ 30K), one that we associate with the $YRuO_4$ layers that indicates static magnetic ordering, the other that we associate with the SrO layers, which exhibits superconducting behavior in transverse field. These results support the hypothesis that the hole condensate is located in the reservoir layers, namely the SrO layers.

These results also imply a picture of this compound, in which there are alternating layers of superconducting and magnetically-ordered material, with the magnetic field lying along the respective plane faces, and alternating in direction. These results are described in detail in reference 16, by D.R. Harshman *et al.* This paper was presented by C.E. Stronach at the *Eighth International Conference on Muon Spin Rotation/Relaxation/Resonance* in August/September 1999, held in Les Diablerets, Switzerland. It is included as an appendix to this report. (D.R. Harshman *et al.*, Physica B 289-290, 360 (2000)).

In addition to the new and exciting results described above, several additional noteworthy results were obtained, submitted or published during this reporting period. A paper on *Coexistence of ferromagnetism and superconductivity in the hybrid ruthenate-cuprate compound* $RuSr_2GdCu_2O_8$ *by muon spin rotation and dc magnetization* (C. Bernhard *et al.*, collaboration with the MPI-Stuttgart and Konstanz group, Phys. Rev. B **59** (1999) 14,099) was published in June 1999 that shows manifestations of this coexistence in μ^+SR data. The zero-field measurements indicate that the ferromagnetic phase is homogeneous on a microscopic scale and accounts for most of the sample volume. Also, the magnetic order appears not to be significantly modified at the onset of superconductivity. This paper is enclosed as an appendix.

A paper on *Low temperature vortex structures in underdoped* $Bi_2Sr_2CaCu_2O_{8+\delta}$ (T. Blasius *et al.*, collaboration with the Konstanz-MPI-Stuttgart group, published in the Proceedings of the Eighth International Conference on Muon Spin Rotation, Relaxation & Resonance, in *Physica B*) describes measurements on the vortex state of Bi-2212 single crystals. We observed a reorganization of the vortex structure with increasing vortex density that appears to be related to a disorder-induced destruction of the vortex lattice. Also, we found evidence for a partial restoration of the vortex lines at higher fields. This may be related to the increase of the vortex-vortex interaction and the subsequent change from single vortex pinning to collective pinning.

A paper on *Melting and dimensionality of the vortex lattice in underdoped* $YBa_2Cu_3O_{6.60}$ was published in Physical Review B. Stronach and Noakes collaborated with J.E. Sonier of Los Alamos National Laboratory, and J.H. Brewer and R.F. Kiefl and associates of the University of British Columbia in this study, which revealed a vortex-lattice melting transition at much lower temperature than in the fully oxygenated material. This suggests that adjacent layers of "pancake" vortex decouple in the liquid phase. In addition, evidence is found for a pinning-induced crossover from a solid 3D to a quasi-2D vortex lattice.

A paper entitled *Zero-field muon-spin-rotation study of hole antiferromagnetism in low-carrier-density* $Y_{1-x}Ca_xBa_2Cu_3O_6$, by Stronach, Noakes, X. Wan (former VSU physics graduate student), and members of the Konstanz-MPI-Stuttgart group was included in the 1998 annual report as a pre-

print. It has since been revised and published (*Physica C 311 (1999) 19*). Based on data taken at TRIUMF, we showed that even in the low-carrier-density regime, the long-range antiferromagnetic ordering is still strongly frustrated by the spin-glass mechanism through calcium doping. Apparent transitions were observed between the frozen-hole antiferromagnetic state and the spin-glassy state. These data made it all the more apparent that the same magnetic interactions hold in both low-carrier-density *(Y,Ca)-123* and *$(La,Sr)_2CuO_4$*.

Range-Correlated Magnetic Moment Variation (RCMMV)

In previously published work, Noakes and collaborators reported a static ZF muon spin relaxation function with anomalously shallow, or even completely absent, minimum before the recovery to 1/3 (of initial asymmetry) in the spin-frozen states of icosahedral Al-Mn-Si [1] quasicrystals and Ce(Ni,Cu)Sn Kondo-semimetal alloys,[2,3] and had developed the phenomenological "Gaussian-broadened Gaussian" static ZF relaxation function that fits those data.[4]

Noakes performed numerical simulations demonstrating that "range-correlated moment-magnitude variation" (RCMMV) can produce arbitrarily-shallow static ZF-μSR functions. The depth of the minimum is an (inverse) indicator of the correlation length, from zero for the standard Gaussian Kubo-Toyabe, to infinite correlation length for monotonic static relaxation. The property varying with a correlation range is surprising, however: it is the magnitude of the ions' local moments. Moment orientation was always completely random (as appropriate for frozen spin glass-like states), but their magnitude also varied, with a correlation length. A paper describing these results has now appeared, which is included as an appendix to this report. (**D.R. Noakes**, J. Phys. Cond. Matter 11, 1589 (1999)) [5]. At the 1999 Int. Conf. on μSR, independent confirmation of this work was provided by the Columbia group, who observed shallow static ZF muon spin relaxation functions in the "two-leg spin-ladder system" $Sr(Cu_{1-x}Zn_x)O_3$, and performed independent numerical simulations arriving at a RCMMV model for the system.[6]

[1] **D.R. Noakes**, A. Ismail, E.J. Ansaldo, J.H. Brewer, G.M. Luke, P. Mendels and S.J. Poon, Phys. Lett. A 199, 107 (1995).

[2] S.J. Flaschin, A. Kratzer, F.J. Burghart, G.M. Kalvius, R. Wäppling, **D.R. Noakes**, R. Kadono, I. Watanabe, T. Takabatake, K. Kobayashi, G. Nakamoto and H. Fujii, J. Phys. Cond. Matter 8, 6967 (1996).

[3] G.M. Kalvius, S.J. Flaschin, T. Takabatake, A. Kratzer, R. Wäppling, **D.R. Noakes**, F.J. Burghart, A. Brückl, K. Neumaier, K. Andres, R. Kadono, I. Watanabe, K. Kobayashi, G. Nakamoto and H. Fujii, Physica B 230-232, 655 (1997).

[4] **D.R. Noakes** and G.M. Kalvius, Phys. Rev. B 56, 2352 (1997).

[5] **D.R. Noakes**, J. Phys. Cond. Matter 11, 1589 (1999)

[6] M.I. Larkin *et al.*, Proc. 1999 Int. Conf. μSR, Physica B 289-290, 153 (2000).

μSR in Rare-Earth Quasicrystals

Quasicrystals are materials that have long-range orientational order without translational periodicity. Only a small number of quasicrystalline materials display any magnetism. Noakes and collaborators had previously published on μSR in spin-glassy icosahedral Al-Mn-Si.[1] In Dec. 1996 and July 1997, they performed μSR measurements of icosahedral Gd-Mg-Zn and Tb-Mg-Zn, both of which show spin-glass behavior in bulk measurements, with spin-freezing temperatures below 10K.

Whereas neutron scattering researchers had reported magnetic "quasi-lattice" ordering at 20K in Tb-Mg-Zn,[3] our μSR spectra showed no evidence of any transition around 20K, seeing instead spin freezing typical of concentrated-moment spin glasses below 10K in both samples. Note that no bulk measurement has indicated any transition near 20K, so the neutron scattering report stands isolated and unconfirmed. The concentrated-spin-glass behavior (temperature-dependent relaxation rate to far above T_g, zero-field (ZF) relaxation rate exceeding instrument resolution below T_g) for 8 magnetic ions per hundred ($RE_8Mg_{42}Zn_{50}$) contrasts with dilute spin-glass behavior (temperature-dependent relaxation only below ~$2T_g$, ZF relaxation resolved at all temperatures) in $Al_{25.5}Mn_{20.5}Si_4$ quasicrystal, where there are 20.5 Mn ions per hundred. This re-enforces the conclusion of the earlier work that only a fraction of the Mn ions are magnetic, and indicates that the magnetism of the rare earth quasicrystals is less anomalous than that of *I*-Al-Mn-Si. Much faster relaxation in the Tb quasicrystal than in the Gd one indicates significant "Crystalline Electric Field" (CEF) effects for the non-S rare earth ions in this structure, but we did not understand at that time why power-exponential ($\exp[-\Lambda t]^p$, where Λ and p are temperature dependent) relaxation, often found in μSR of concentrated-moment spin glasses above T_g, occurs only in the Tb sample here, not the Gd one. This question was resolved in 2002.

While the ZF-μSR became too fast to measure below T_g in both samples, we did observe longitudinal-field (LF) partial decoupling in applied fields up to 2 Tesla at dilution refrigerator temperatures, and were able to fit the spectra to a model of a very-nearly static Gaussian field distribution, consistent with our dense spin glass description. These results were published in Physics Letters A. [2] This paper is included as an appendix to this report.

[1] **D.R. Noakes**, A. Ismail, E.J. Ansaldo, J.H. Brewer, G.M. Luke, P. Mendels and S.J. Poon, Phys. Lett. A 199, 107 (1995).

[2] **D.R. Noakes**, G.M. Kalvius, R. Wäppling, **C.E. Stronach, M.F. White**, H. Saito and K. Fukamichi, Phys. Lett. A 238, 197 (1998).

[3] B. Charrier, B. Ouladdiaf and D. Schmitt, Phys. Rev. Lett. 78, 4637 (1997).

Magnetic Frustration and Competing Exchange

Frustration of, or competition between, magnetic ordering interactions can reduce ordering temperatures, can cause complicated magnetic ordering structures, and can cause anomalous magnetic dynamics above the ordering temperatures. In beginning to study these effects with μSR, we have done experiments on:

$GdMn_2$, where the Mn sub-lattice is frustrated but the Gd lattice is not. Our μSR is providing new information on the several ordered states,[1] which are not well understood, partly because Gd absorbs so many neutrons that neutron diffraction is difficult to do.

YMn_{12}, a transition-moment-only baseline material for comparison to $REMn_{12}$, $REFe_4Al_8$ and $REFe_6Al_6$ competing-exchange materials, which all have in fact the same crystal structure. In spite of three crystallographically-distinct Mn sites with two different moments in the ordered state,[2] our paper presented at the 1999 Int. Conf. μSR [3] shows that well below T_N ZF muon spin relaxation is fairly slow and characteristic of a Lorentzian field distribution (there is no coherent oscillation), indicating near-perfect cancellation of all local fields at the muon. Noakes has used his muon site-search software [4] to identify the likely interstitial muon sites as the unit cell positions (0,½,¼) and (0,0,½). These are both high-symmetry sites for which Noakes has now demonstrated that the dipole field sum at both these sites for the published magnetic structure is zero. With this site identification, μSR in YMn_{12} is understood. The site identification extends to the competing-exchange materials with magnetic rare earths, which should make interpretation of μSR in them easier, as well.

$TbFe_6Al_6$ and $ErFe_6Al_6$, *d*-band *vs.* RKKY competing exchange materials. The very rapid relaxation caused by the large rare earth moments limits the amount of information that can be extracted reliably from μSR, but there are clear indications of substantial spin dynamics affecting the muon relaxation in the wide range of temperature where bulk magnetization indicates that the ferrimagnetic moment does not develop in a standard Brillouin-curve manner.[5]

$TbCo_xNi_{1-x}C_2$, which is a competing exchange system in the sense that the magnetic ordering switches from antiferromagnetic for Ni-rich to ferromagnetic for Co-rich but the transition ions themselves are non-magnetic, so there is only the RKKY interaction. For intermediate values of x there are two magnetic transitions as temperature is lowered, with a modulated antiferromagnetic structure at the lowest temperatures. In the intermediate-x alloys, μSR sees considerable local spin disorder and dynamics at all temperatures and in all the magnetic states.[6]

[1] E.M. Martin, E. Schreier, G.M. Kalvius, A. Kratzer, O. Hartmann, R. Wäppling, **D.R. Noakes**, K. Krop, R. Ballou and J. Deportes, Physica B 289-290, 265 (2000).

[2] J. Deportes and D. Givord, Solid State Commun. 19, 845 (1976).

[3] G.M. Kalvius, K.H. Münch, A. Kratzer, R. Wäppling, **D.R. Noakes**, J. Deportes and R. Ballou, 1999 International Conference on Muon Spin Relaxation, Physica B.289-290, 261 (2000).

[4] **D.R. Noakes**, J.H. Brewer, D.R. Harshman, E.J. Ansaldo, and C.Y.Huang, Phys. Rev. B 35, 6597 (1987).

[5] G.M. Kalvius, **D.R. Noakes**, G. Grosse, W. Schäfer, W. Kockelmann, S. Fredo, I. Halevy and J. Gal, Physica B 289-290, 225 (2000).

[6] G.M. Kalvius, **D.R. Noakes**, R. Wäppling, G. Grosse, W. Schäfer, W. Kockelmann, J.K. Jakinthos, and P.A. Kotsanides, Physica B 326, 465 (2003).

Mechanical Milling

This project, as originally proposed to the Air Force Office of Scientific Research, contained a mechanical-milling component, which involved development of a laboratory at Virginia State University to produce and characterize nanostructured iron alloys. Dr. Anthony S. Arrott, Professor Emeritus from Simon Fraser University, joined the VSU faculty as a part-time Distinguished Senior Research Professor to provide scientific direction for this part of the research program in February 1998. Shortly after this program was funded, a separate grant from the Ballistic Missile Defense Organization funded the mechanical milling program. Details of the accomplishments of this program are given in its annual reports, which were submitted to the Air Force Office of Scientific Research (F49620-97-1-0532) and the Ballistic Missile Defense Organization.

This program was continued with support from another grant from the AFOSR as the Iron Alloys Research Program, through which three major discoveries were subsequently made in 2002-03: spin-density waves in Fe(Al) alloys, magnetic foam, and inverse melting.

Magnetism Laboratory

A proposal, *Magnetic Materials Laboratory Development*, submitted to the FY 99 DOD HBCU/MI Infrastructure Support Program, was funded for $194,540 plus $5,000 matching funds by Virginia State University, effective September 1, 1999. This grant has enabled the VSU researchers to develop a magnetometer system of unprecedented sensitivity. Equipment purchased includes a cryofree superconducting split-coil magnet, a Compumotor linear servo drive, a sensitive digital voltmeter, a differential scanning calorimeter, a bipolar power supply, and a precision LCR meter.

This laboratory is focused primarily on the fabrication and characterization of nanostructured iron alloys, which is conducted by Dr. Anthony S. Arrott, Distinguished Senior Research Professor of Physics, Stronach, Noakes and students.

In addition to the equipment to be purchased through this grant, Arrott has obtained, as a gift from the Honeywell Corporation, a 2.0-Tesla Walker Scientific electromagnet, which plays an important role in the magnetic measurements planned for this laboratory. The faculty participating in this project include Stronach, Arrott, Noakes, and George W. Henderson, Assistant Professor of Physics.

International Muon Spin Rotation Conference

As is noted at several places in this report, Stronach and Noakes attended the *Eighth International Conference on Muon Spin Rotation/Relaxation/Resonance*, which was held in Les Diablerets, Switzerland, August 30 - September 3, 1999. They presented a number of papers, to which references are made in this report. It should also be noted that Stronach, who was a member of the *International Advisory Committee on Muon Spin Rotation*, issued an invitation to the group to hold the 2002 conference in Virginia. The invitation was accepted, and the precise location was later chosen to be Williamsburg. Stronach and Noakes were named chairman and secretary, respectively.

Publications in Refereed Journals

[1] J.E.Sonier, J.H. Brewer, R.F. Kiefl, D.A. Bonn, S.R. Dunsiger, W.N. Hardy, R. Liang, W.A. MacFarlane, R.I. Miller, T.M. Riseman, *μSR measurement of the fundamental length scales in the vortex state of $YBa_2Cu_3O_{6.60}$*, **D.R. Noakes, C.E. Stronach**, and **M.F. White, Jr.**, Phys. Rev. Lett. 79, 2875 (1997).

[2] **D.R. Noakes**, E. Fawcett and T.M. Holden, *Concentration dependence of critical scattering from Cr(V) alloys above the Néel temperature*, Phys. Rev. B 55, 12504 (1997).

[3] G.M. Kalvius, S.J. Flaschin, T. Takabatake, A. Kratzer, R. Wäppling, **D.R. Noakes**, F.J. Burghart, A. Brückl, K. Neumaier, K. Andres, R. Kadono, I. Watanabe, K. Kobayashi, G. Nakamoto and H. Fujii, *μSR studies of magnetic correlations in Pt and Cu-doped CeNiSn*, Physica B 230-232, 655 (1997).

[4] **D.R. Noakes** and G.M. Kalvius, *Anomalous zero-field muon spin relaxation in highly disordered magnets*, Phys. Rev. B Brief Reports 56, 2352 (1997).

[5] A. Kratzer, G.M. Kalvius, S.J. Flaschin, **D.R. Noakes**, R. Wäppling , A. Brückl, K. Neumaier, K. Andres, T. Takabatake, K. Kobayashi, G. Nakamoto and H. Fujii, *μSR magnetic response of CeNiSn on impurity content*, Physica B 230-232, 661 (1997).

[6] **D.R. Noakes**, E. Fawcett, B.J. Sternlieb, G. Shirane and J. Jankowska, *Nature of the triple point in chromium alloys: mode-softening of the incommensurate spin density wave*, Physica B 241-243, 625 (1998).

[7] **D.R. Noakes**, G.M. Kalvius, R. Wäppling, **C.E. Stronach, M.F. White**, H. Saito and K. Fukamichi, *Spin dynamics and freezing in magnetic rare-earth quasicrystals*, Phys. Lett. A 238, 197 (1998).

[8] R.I. Grynszpan, I. Savic, S. Romer, X. Wan, J. Fenichel, C.M. Aegerter, H. Keller, **D.R. Noakes**, **C.E. Stronach**, A. Maignan, C. Martin and B. Raveau, *Temperature dependence of the muon spin relaxation in $Pr_{½}Sr_{½}MnO_3$*, Physica B 259-261, 824 (1999).

[9] C. Bernhard, J.L. Tallon, C. Niedermayer, T. Blasius, A. Golnik, E. Brücher, R.K. Kremer, **D.R. Noakes**, **C.E. Stronach** and E.J. Ansaldo, *Coexistence of ferromagnetism and superconductivity in the hybrid ruthenate-cuprate compound $RuSr_2GdCu_2O_8$ studied by muon spin rotation and DC magnetization*, Physical Review B **59**, 14099 (1999).

[10] **D.R. Noakes**, *A correlation length measured by zero-field muon spin relaxation in disordered magnets*, Journal of Physics: Condensed Matter **11**, 1589 (1999).

[11] **C.E. Stronach, D.R. Noakes, X. Wan**, C. Niedermayer, C. Bernhard and E.J. Ansaldo, *Zero-field muon spin rotation study of hole antiferromagnetism in low-carrier-density* $Y_{1-x}Ca_xBa_2Cu_3O_6$, Physica C **311**, 19 (1999).

[12] J.E. Sonier, R.F. Kiefl, J.H. Brewer, D.A. Bonn, S.R. Dunsiger, W.N. Hardy, R. Liang, W.A. MacFarlane, T.M. Riseman, **D.R. Noakes** and **C.E. Stronach**, *Expansion of the vortex cores in* $YBa_2Cu_3O_{6.95}$, Physical Review B Rapid Communications **59**, R729 (1999).

[13] X. Wan, W.J. Kossler, **C.E. Stronach** and **D.R. Noakes**, "Cauchy magnetic field component and magnitude distribution studied by the zero-field muon spin relaxation technique", Hyperfine Interactions 122, 233 (1999).

[14] D.R. Harshman, W.J. Kossler, A.J. Greer, **C.E. Stronach**, E. Koster, B. Hitti, M.K. Wu, D.Y. Chen, F.Z. Chien, *Muon spin rotation in* $Sr_2YRu_{1-x}Cu_xO_{6-\delta}$, Proceedings of the 2nd Annual Conference on New Theories, Discoveries, and Related Applications of Superconductors and Related Materials (1999), International Journal of Modern Physics B **13** (1999) 3670.

[15] H.A. Blackstead, J.D. Dow, D.R. Harshman, M.J. DeMarco, M.K. Wu, D.Y. Chen, F.Z. Chien, D.B. Pulling, W.J. Kossler, A.J. Greer, **C.E. Stronach**, E. Koster, B. Hitti, M. Haka, S. Toorongian, *Magnetism and superconductivity in* $Sr_2YRu_{1-u}Cu_uO_6$ *and magnetism in* $Ba_2GdRu_{1-u}Cu_uO_6$, European Journal of Physics B **15** (2000) 649.

[16] D.R. Harshman, W.J. Kossler, A.J. Greer, **C.E. Stronach**, E. Koster, B. Hitti, M.K. Wu, D.Y. Chen, F.Z. Chien, H.A. Blackstead, J.D. Dow, *Location of the superconducting hole condensate in* $Sr_2YRu_{1-u}Cu_uO_6$ *by* μ^+SR, Physica B **289-290** (2000) 360.

[17] G.M. Kalvius, **D.R. Noakes**, G. Grosse, W. Schäfer, W. Kockelmann, S. Fredo, I. Halevy and J. Gal, *Magnets frustrated by competing exchange (*$TbFe_6Al_6$ *and* $ErFe_6Al_6$*)*, Proceedings 1999 International Conference on Muon Spin Relaxation, Physica B 289-290, 225 (2000).

[18] **D.R. Noakes** and G.M. Kalvius, *Spin-slip structure induced by the crystalline electric field in the incommensurate magnetic ordering of CePtSn*, Proceedings 1999 International Conference on Muon Spin Relaxation, Physica B 289-290, 248 (2000).

[19] G.M. Kalvius, A. Kratzer, H. Nakotte, **D.R. Noakes, C.E. Stronach** and R. Wäppling, *μSR magnetic response of CeCuSn*, Proceedings 1999 International Conference on Muon Spin Relaxation, Physica B 289-290, 252 (2000).

[20] G.M. Kalvius, A. Kratzer, G. Grosse, **D.R. Noakes**, R. Wäppling, H. v. Löhneysen, T. Takabatake and Y. Echizen, *The onset of magnetism in* $CeNi_{1-x}T_xSn$ *(T=Cu,Pt)*, Proceedings 1999 International Conference on Muon Spin Relaxation, Physica B 289-290, 256 (2000).

[21] G.M. Kalvius, K.H. Münch, A. Kratzer, R. Wäppling, **D.R. Noakes**, J. Deportes and R. Ballou, *μSR study of* YMn_{12}, Proceedings 1999 International Conference on Muon Spin Relaxation, Physica B 289-290, 261 (2000).

[22] E.M. Martin, E. Schreier, G.M. Kalvius, A. Kratzer, O. Hartmann, R. Wäppling, **D.R. Noakes**, K. Krop, R. Ballou and J. Deportes, *Magnetic properties of $GdMn_2$ from μSR*, Proceedings 1999 International Conference on Muon Spin Relaxation, Physica B 289-290, 265 (2000).

[23] F.J. Burghart, W. Potzel, G.M. Kalvius, E. Schreier, G. Grosse, **D.R. Noakes**, W. Schäfer, W. Kockelmann, S.J. Campbell, W.A. Kaczmarek, A. Martin and M.K. Krause, *Magnetism of crystalline and nanostructured $ZnFe_2O_4$*, Proceedings 1999 International Conference on Muon Spin Relaxation, Physica B 289-290, 286 (2000).

[24] **D.R. Noakes**, R. Wäppling, G.M. Kalvius, Y. Andersson, A. Broddefalk, **M.F. White** and **C.E. Stronach**, *μSR magnetic response of stoichiometric and non-stoichiometric PrP*, Proceedings 1999 International Conference on Muon Spin Relaxation, Physica B 289-290, 303 (2000).

[25] T. Blasius, C. Niedermayer, D.M. Pooke, **D.R. Noakes**, **C.E. Stronach**, E.J. Ansaldo, A. Golnik and C. Bernhard, *Low temperature vortex structures of the mixed state in underdoped $Bi_2Sr_2CaCu_2O_{8-\delta}$*, Proceedings 1999 International Conference on Muon Spin Relaxation, Physica B 289-290, 265 (2000).

[26] J.E. Sonier, J.H. Brewer, R.F. Kiefl, D.A. Bonn, J. Chakhalian, S.R. Dunsiger, W.N. Hardy, R. Liang, W.A. MacFarlane, R.I. Miller, **D.R. Noakes**, T.M. Riseman, and **C.E. Stronach**, *Melting and dimensionality of the vortex lattice in $YBa_2Cu_3O_{6.60}$*, Phys. Rev. B Rapid Commun. **61**, R890 (2000).

---

[27] L. Heilbronn, **R.S. Cary**, M. Cronqvist, F. Deák, K. Frankel, A. Galonsky, K. Holabird, Á. Horvath, Á. Kiss, J. Kruse, R. Ronningen, H. Schelin, Z. Seres, **C.E. Stronach**, J. Wang, P. Zecher and C. Zeitlin, *Neutron yields from 155 MeV/nucleon C and He stopping in Al*, Nuclear Science and Engineering **132** (1999) 1. (no AFOSR support involved)

Student Activities

Ceasar U. Jackson, Jr. completed his studies and received the Master of Science degree in physics at the May 2000 commencement exercises at Virginia State University. His thesis is titled "Muon Spin Rotation Study of the Anomalous *f*-electron Compound Ce_7Ni_3".

Morris F. White, Jr. completed his thesis, "Numerical Investigations of Novel Observed Muon Spin Relaxation Functions", in December 2000, and received his Master of Science degree in May 2001.

Both Jackson and White visited the TRIUMF laboratory twice to obtain data for their theses. White's travel expenses were covered by his employer, Philip Morris, USA.

Three undergraduates, Larry Harris, Jerrod Spencer, and Mensah Alkebu-lan participated in the research program and graduated with Bachelor of Science degrees in physics. Harris then attended Clemson University, where he received his Master of Science degree in May 2003. Spencer was tragically killed in an automobile accident in early 2003.

Appendices

Four of the 26 papers published with support from AFOSR grant F49620-97-1-0297 are attached as appendices to this report. They were chosen because they represent the scientific findings with the greatest impact that this group published as a direct consequence of this support. The term "direct consequence" is used because this support for the magnetism research team at Virginia State University has led to many additional important findings, and we are confident that many more are yet to come.

The attached papers are:

[1] D.R. Harshman, W.J. Kossler, A.J. Greer, **C.E. Stronach**, E. Koster, B. Hitti, M.K. Wu, D.Y. Chen, F.Z. Chien, H.A. Blackstead, J.D. Dow, *Location of the superconducting hole condensate in* $Sr_2YRu_{1-u}Cu_uO_6$ *by* μ^+SR, Physica B **289-290**, 360 (2000).

[2] C. Bernhard, J.L. Tallon, C. Niedermayer, T. Blasius, A. Golnik, E. Brücher, R.K. Kremer, **D.R. Noakes, C.E. Stronach** and E.J. Ansaldo, *Coexistence of ferromagnetism and superconductivity in the hybrid ruthenate-cuprate compound* $RuSr_2GdCu_2O_8$ *studied by muon spin rotation and DC magnetization*, Physical Review B **59**, 14099 (1999).

[3] D.R. Noakes, *A correlation length measured by zero-field muon spin relaxation in disordered magnets*, Journal of Physics: Condensed Matter **11**, 1589 (1999).

[4] D.R. Noakes, G.M. Kalvius, R. Wäppling, **C.E. Stronach, M.F. White**, H. Saito and K. Fukamichi, *Spin dynamics and freezing in magnetic rare-earth quasicrystals*, Phys. Lett. A 238, 197 (1998).

In addition, the first page and table of contents are included of a massive article that was later published in the *Handbook on the Physics and Chemistry of Rare Earths, Vol. 32*. The authors are G.M. Kalvius, **D.R. Noakes**, and O. Hartmann.

APPENDICES

ELSEVIER

Physica B 289–290 (2000) 360–364

PHYSICA B

www.elsevier.com/locate/physb

Location of the superconducting hole condensate in $Sr_2YRu_{1-u}Cu_uO_6$ by μ^+SR

D.R. Harshman[a,b,*], W.J. Kossler[c], A.J. Greer[d], C.E. Stronach[e], E. Koster[f], B. Hitti[g], M.K. Wu[h], D.Y. Chen[h,*], F.Z. Chien[i], H.A. Blackstead[b], John D. Dow[j]

[a]*Physikon Research, Inc., P.O. Box 2421, Blaine, WA 98231, USA*
[b]*Department of Physics, University of Notre Dame, Notre Dame, IN 46556, USA*
[c]*Department of Physics, College of William and Mary, Williamsburg, VA 23187, USA*
[d]*Department of Physics, Gonzaga University, Spokane, WA 99258, USA*
[e]*Department of Physics, Virginia State University, Petersburg, VA 23806, USA*
[f]*Department of Physics, University of British Columbia, Vancouver, B.C., Canada V6T 1Z1*
[g]*TRIUMF, Vancouver, B.C., Canada V6T 2A3*
[h]*Department of Physics & Materials Science Center, National Tsing Hua University, Hsinchu, Taiwan*
[i]*Department of Physics, Tamkang University, Tansui, Taiwan*
[j]*Department of Physics, Arizona State University, Tempe, AZ 85287, USA*

Abstract

The magnetic and superconducting characteristics of sintered $Sr_2YRu_{1-u}Cu_uO_6$ (for $u = 0.05, 0.10, 0.15$) were probed using transverse- and zero-field muon-spin rotation (μ^+SR). Since positive muons are attracted to oxygen ions in the high-T_C oxides, $Sr_2YRu_{1-u}Cu_uO_6$ should (and does) present two types of μ^+ sites, one in the $YRuO_4$ layers and the other in the SrO layers. The transverse- and zero-field μSR spectra for all three stoichiometries exhibit magnetic ordering at and below $T_N \approx 30$ K, with a static local field of ~ 3 kG. This transition is marked by a dramatic increase in the μ^+ spin relaxation rate as the temperature decreases below T_N, corresponding to an increased static disordering of the magnetic moments. Above T_N no static fields are observed. Instead, the data exhibit a slow dynamic depolarization, presumably due to rapid fluctuation of magnetic moments. Both transverse- and zero-field data also indicate a smaller second component ($\sim 10\%$) that we associate with the SrO layer, exhibiting superconducting behavior in transverse field with an observed bulk $T_C \approx T_N \sim 30$ K.

Keywords: Superconductivity; Antiferromagnetism; Muon spin rotation

High-T_C superconductivity has (in the past) generally been associated with the perovskite structures containing CuO_2 planes. However, it has been suggested that CuO_2 planes are not necessary for high-T_C superconductivity. Indeed, some organic superconductors are included in the growing list of high-T_C superconductors [1,2]. In this work, we describe a detailed study of the magnetic order and superconductivity of the Cu-doped $Sr_2YRu_{1-u}Cu_uO_6$ system ($u = 0.05$, 0.10, 0.15) with so little Cu that CuO_2 planes do not form (see Fig. 1). In the high-T_C oxides the implanted μ^+

*Corresponding author. P.O. Box 2421, Blaine, WA 98231, USA. Tel.: + 1-360-354-8521; fax: + 1-360-354-8521.
E-mail address: drh@physikon.net (D.R. Harshman).
*Deceased.

0921-4526/00/$ - see front matter
PII: S0921-4526(00)00411-7

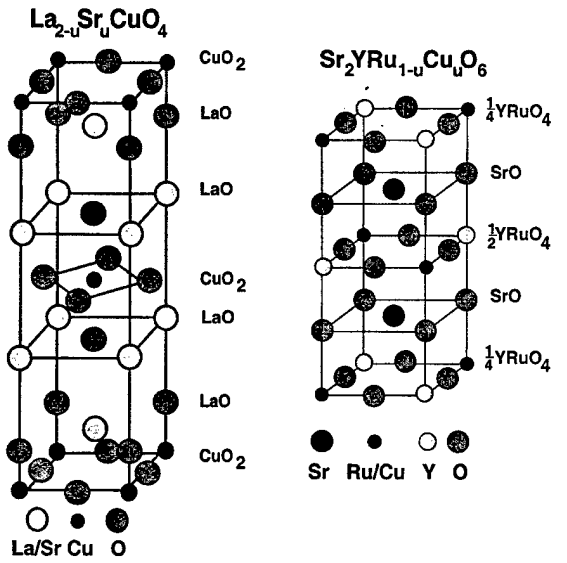

Fig. 1. On the right is the crystal structure of $Sr_2YRu_{1-u}Cu_uO_6$. Two nearly equivalent oxygen sites in the $YRu_{1-u}Cu_uO_4$ layer are designated O(1) and O(2), and the O(3) site is in the SrO layer. On the left is the crystal structure of $La_{2-u}Sr_uCuO_4$ for comparison.

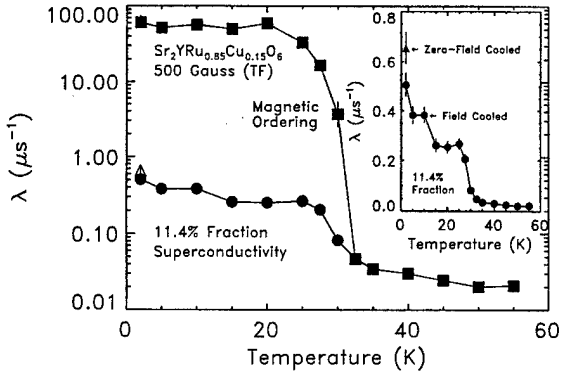

Fig. 2. The exponential relaxation rate λ versus temperature for the $\mu_{O(1,2)}$ (squares) and $\mu_{O(3)}$ (circles) sites. The triangles represent data taken by first zero-field cooling and then applying the 500 G transverse field. The inset shows $\lambda(T)$ for the $\mu_{O(3)}$ site on a linear scale. The lines connecting the data are to guide the eye.

particles tend to be trapped near the oxygen sites [3]. In the case of Sr_2YRuO_6, there are three inequivalent oxygen sites: Two in the $YRuO_4$ layer [designated O(1,2), because the O(1) and O(2) sites are only slightly different], and one in the SrO layer [designated O(3)]. There are correspondingly two muon sites available. One is formed by four (two O(1) and two O(2)) oxygens in the $YRu_{1-u}Cu_uO_4$ layer, designated the $\mu_{O(1,2)}$-site. The second site, associated with the SrO layer and designated the $\mu_{O(3)}$-site, is also formed by four oxygens, two O(3) and an O(1) and an O(2). The volume available to the muon at each of these sites is roughly commensurate with the size of muonium. Thus we expect to see a two-component muon-spin relaxation spectrum.

Polycrystalline samples of $Sr_2YRu_{1-u}Cu_uO_6$ were prepared by the standard solid-state reaction method [4]. Structural characterization was carried out with an energy dispersive X-ray analyzer, by high-resolution X-ray diffraction, and by neutron scattering — confirming that the samples have the Sr_2YRuO_6 stoichiometry and phase homogeneity. The upper limit of the amount of impurity phase is estimated to be less than 1%. The standard time-differential μ^+SR technique was employed, utilizing the M20 beam line at the TRIUMF accelerator [5,6]. Our spectrometer incorporates a veto system that virtually eliminates background signals from muons that miss the sample, which greatly facilitates the recovery and separation of a minority signal. In this work, we utilize the local-probe nature of the μ^+SR technique to obtain microscopic evidence for the existence of bulk superconductivity in this material, which on the one hand is magnetic and on the other superconducts although it possesses neither CuO nor CuO_2 planes.

Figs. 2 and 3 show the transverse-field relaxation rate λ and precession frequency ν versus temperature for $u = 0.15$ ($u = 0.05$ and 0.10 show similar behavior). At temperatures below ~ 30 K, both the zero-field (ZF) and transverse-field (TF) spectra indicate two components, designated $\mu_{O(1,2)}$ and $\mu_{O(3)}$, reflecting the expected two distinct muon sites. The subscripts correspond to the oxygen in the $YRuO_4$ layers and the oxygen in the SrO layers, respectively. In ZF, the $\mu_{O(1,2)}$ site ($\sim 90\%$ of total signal amplitude) exhibits fast relaxation and a large (~ 3 kG) local magnetic field, while the $\mu_{O(3)}$ site ($\sim 10\%$ of total amplitude) shows neither significant relaxation nor a locally ordered field.

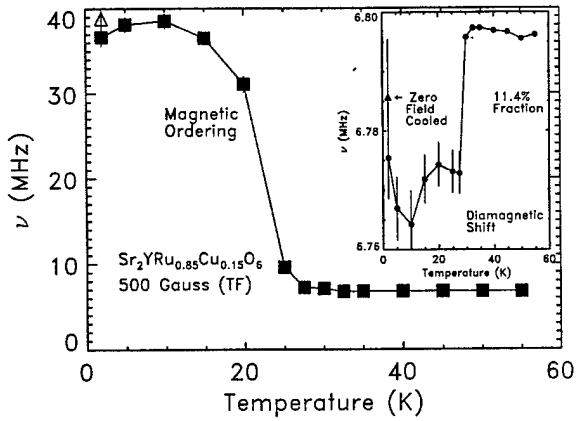

Fig. 3. The muon precession frequency versus temperature for the $\mu_{O(1,2)}$ (squares) and $\mu_{O(3)}$ (inset – circles) sites. The triangles represent data taken by zero-field cooling and then applying the 500 G transverse field. The lines connecting the data points are to guide the eye.

From these data, the spin-freezing temperature, T_N, appears to be ~ 30 K. At low temperatures, the 3 kG local field at the $\mu_{O(1,2)}$ muon site is necessarily associated with the ordering of the Ru moments. Moreover, the very fast relaxation of the muon ensemble at the $\mu_{O(1,2)}$ site reflects a strong disordering of the Ru moments as well. When combined with recent polarized neutron data [7], a picture of in-plane freezing of Ru spins with the average polarization reversing direction from one $YRuO_4$ layer to the next emerges, thereby presenting a zero field at the $\mu_{O(3)}$ site in the SrO layer. Above ~ 30 K relaxation due to static electronic moments disappears, suggesting motional narrowing of the lines due to rapid fluctuations of the Ru moments.

Upon application of a 500 G transverse field, the $\mu_{O(1,2)}$ site again displays rapid μ^+ spin depolarization and large local magnetic field, while the $\mu_{O(3)}$ site clearly exhibits à 10-fold rise in the relaxation rate λ as temperature decreases from 30 to 2 K, along with a concomitant diamagnetic shift – consistent with superconductivity. Exponential depolarization forms $[\exp(-\lambda t)]$ were assumed in analyzing both signals. An additional DC offset was included since the applied field was much smaller than the local field. Note the relative increase in λ at 2 K for the $\mu_{O(3)}$ site after zero-field cooling (ZFC – see inset of Fig. 2). This is an expected consequence of an induced increase in the spatial disorder of the superconducting vortices. Interestingly, when the magnetic field is removed in a field-cooled sample, we see little evidence of trapped flux, indicating very weak flux pinning. This may be related to having essentially zero vortex coupling between superconducting layers, i.e., isolated sheets of "pancake" vortices, which is consistent with having the superconducting hole condensate residing in the SrO layers. Thus, fully developed bulk superconductivity forms below $T_N \sim 30$ K (i.e., when static magnetic order is seen at the $\mu_{O(1,2)}$ site).

We now compare our data with two competing models. The dominant fact about this material is that superconductivity and magnetism co-exist in the same unit cell (not necessarily in the same layer). The Ren–Wu p-wave pairing model [8–10] has ferromagnetic coupling by double exchange between adjacent Ru spins [11,12], and was solved in a molecular-field approximation by de Gennes [13,14]. The magnetic properties are determined by J, the AFM exchange, and b, the inter-layer double exchange. Monte Carlo calculations revealed that, for a given strength of the interlayer double exchange, two magnetically ordered states can be encountered as the temperature is lowered: (i) antiferromagnetic order (for $T_1 < T < T_N$) followed by canting (for $T < T_1$), or (ii) ferromagnetic order (for $T_1 < T < T_F$) followed by canting (for $T < T_1$). Here, T_1 is the spin-canting temperature, T_F is the ferromagnetic order temperature, and T_N is the Néel temperature. Significant predictions of this picture are (i) that the superconductivity (SC) will have odd parity and p-wave symmetry, and (ii) the current-carrying holes of SC will reside primarily in the $YRuO_4$ layers. However, the requisite canting behavior has not been observed [7]; this picture remains unsupported by experiments.

The charge-reservoir oxygen model (see e.g. Ref. [15–20]), on the other hand, assigns the hole condensate to the reservoir layers, namely the SrO layers in these materials. Its pairing is conventional BCS-like (in all likelihood, s-wave or extended s-wave), but allows for electronic as well as phononic pairing. It also embraces the bond-valence-sum

calculations [21–25] for the ionic charges, which put the holes in the SrO layers. Significant predictions of this model include: (i) provided that Gd does not order at a high temperature, $Ba_2GdRu_{1-u}Cu_uO_6$ should *not* superconduct, due to pair-breaking by *paramagnetic* $L = 0$ Gd; (ii) the under-charged oxygen ions that carry the primary supercurrent are in the SrO layers, where there is no large average magnetic field; (iii) the μ^+SR signal amplitude from the SrO layers will be weaker than the signal amplitude from the $YRuO_4$ layers, because the holes (repulsive to μ^+) reside (primarily) in the SrO layers where the oxygen ions are not fully charged to O^{-2} [15–20]; and (iv) the carriers of SC are holes and so the Hall coefficient should be positive (hole-like). The present results support this model.

In summary, our data indicate that the $\mu_{O(1,2)}$ site should be associated with oxygens in the $YRuO_4$ layers and the $\mu_{O(3)}$ site with the SrO layers. The marked difference in the μ^+ trapping probabilities between the two sites can be understood as due to a reduced negative charge on the SrO oxygen: this is where the current-carrying holes reside. Muons stopped near oxygen ions in the SrO layers give evidence for vortices below ~ 30 K, as revealed by enhanced disorder seen in the TF data after ZFC at low temperature. We suggest that it may not be a coincidence that the in-plane static magnetic ordering of the Ru moments and the observed fully developed superconductivity in the SrO layers both occur at ~ 30 K. We further posit that the intrinsic T_C (i.e., in the absence of fluctuating magnetic moments) of the superconducting condensate may be higher, but the rapid fluctuations of the Ru moments above T_N may suppress the superconducting state. Note that microwave measurements reported elsewhere [26][1] indicate flux dissipation above 30 K. When the temperature is decreased below T_N, the fluctuations cease and the in-plane magnetic ordering (with average polarization reversing direction from one $YRuO_4$ layer to the next) is established. This unique magnetic state (which provides a zero *net* magnetic field in the SrO layers) may no longer inhibit hole pairing, but does result in the observed fully developed superconductivity in the SrO layers. Our results, along with recent polarized neutron scattering data [7], are consistent with a ferromagnetic $YRu_{1-u}Cu_uO_4$ layer (the data show a broadened field distribution) in which the magnetization vector lies in the a–b plane and reverses direction from magnetic layer to magnetic layer producing a net antiferromagnetic ordering. While these results are completely consistent with the predictions of the charge-reservoir oxygen model [15–20], we cannot absolutely rule out the possibility of exotic superconductivity with higher-order pairing in the $YRuO_4$ layers.

We thank S.R. Kreitzman, D. Arseneau and M. Good for technical support. This research was supported in part by Physikon Research Inc., project PL11-206, and by the US Air Force Office of Scientific Research through grant no. F49620-97-1-0297. M.K.W., D.Y.C., and F.Z.C. gratefully acknowledge the support of the ROC National Science Council Grant NSC87-2212-M-110-006; H.A.B. thanks the US Department of Energy (MISCON) (Grant No. DE-FG02-90ER45427): and J.D.D. thanks the US Army Research Office (Contract DAAG55-97-1-0387).

References

[1] D.R. Harshman, A.P. Mills Jr., Phys. Rev. B 45 (1992) 10684.
[2] D.R. Harshman, A.T. Fiory, R.C. Haddon, M.L. Kaplan, T. Pfiz, E. Koster, I. Shinkoda, D.Ll. Williams, Phys. Rev. B 49 (1994) 12990.
[3] D.R. Harshman, G. Aeppli, G.P. Espinosa, A.S. Cooper, J.P. Remeika, E.J. Ansaldo, T.M. Riseman, D.Ll. Williams, D.R. Noakes, B. Ellman, T.F. Rosenbaum, Z. Physik 38 (1988) 852.
[4] M.K. Wu, D.Y. Chen, F.Z. Chien, S.R. Sheen, D.C. Ling, C.Y. Tai, J.L. Tseng, D.H. Chen, F.C. Zhang, Z. Physik 102 (1997) 37.
[5] A. Schenck, Muon Spin Rotation Spectroscopy, Hilger, Bristol, 1985.
[6] S.F.J. Cox, J. Phys. C 20 (1987) 3187.
[7] D. Y. Chen, M. K. Wu, C-H. Du, P. D. Hatton, F. Z. Chien and C. Ritter, in preparation. .
[8] H. C. Ren and M. K. Wu, unpublished (cond-mat/9805094).
[9] D.Y. Chen, F.Z. Chien, D.C. Ling, J.L. Tseng, S.R. Sheen, M.J. Wang, M.K. Wu, Physica C 282–287 (1997) 73.

[1] Microwave measurements on the same samples indicate an onset T_C of 42.5 K.

[10] M. K. Wu and D. Y. Chen, Physica B 289–290 (2000), these proceedings.
[11] C. Zener, Phys. Rev. 82 (1951) 403.
[12] P.W. Anderson, H. Hasegawa, Phys. Rev. 100 (1955) 675.
[13] P.G. de Gennes, Phys. Rev. 118 (1960) 141.
[14] P.G. de Gennes, C. R. Acad. Sci. 305 (1987) 345.
[15] H.A. Blackstead, J.D. Dow, Phys. Rev. B 51 (1995) 11830.
[16] H.A. Blackstead, J.D. Dow, J. Appl. Phys. 83 (1998) 1540.
[17] H.A. Blackstead, J.D. Dow, Phys. Rev. B 57 (1998) 10798.
[18] H. A. Blackstead and J. D. Dow, in: I. Bozovic, D. Pavuna (Eds.), Oxide Superconductor Physics and Nanoengineering II, Proc. SPIE 2697,1996, p. 120.
[19] J. D. Dow, in: M. Razeghi (Ed.),Photodetectors: Materials and Devices II, Proc. SPIE 2999, 1997, p. 335.
[20] H.A. Blackstead, J.D. Dow, Philos. Mag. 73 (1996) 223.
[21] D. Brown, D. Altermatt, Acta Crystallogr. B 41 (1985) 244.
[22] D. Altermatt, I.D. Brown, Acta Crystallogr. B 41 (1985) 241.
[23] D. Brown, J. Solid State Chem. 82 (1989) 122.
[24] D. Brown, K.K. Wu, Acta Crystallogr. B 32 (1976) 1957.
[25] D. Brown, in: M. O'Keefe, A. Navrotsky (Eds.), Structure and Bonding in Crystals, Vol. II, Academic Press, New York, 1980, pp. 1–20.
[26] H. A. Blackstead, J. D. Dow, D. R. Harshman, M. J. DeMarco, M. K. Wu, D. Y. Chen, F. Z. Chien, D. B. Pulling, W. J. Kossler, A. J. Greer, C. E. Stronach, E. Koster, B. Hitti, M. Haka and S. Toorongian, in preparation.

Coexistence of ferromagnetism and superconductivity in the hybrid ruthenate-cuprate compound $RuSr_2GdCu_2O_8$ studied by muon spin rotation and dc magnetization

C. Bernhard
Max-Planck-Institut für Festkörperforschung, Heisenbergstrasse 1, D-70569 Stuttgart, Germany

J. L. Tallon
Industrial Research Ltd., P. O. Box 31310, Lower Hutt, New Zealand

Ch. Niedermayer and Th. Blasius
Universität Konstanz, Fakultät für Physik, D-78434, Konstanz, Germany

A. Golnik,* E. Brücher, and R. K. Kremer
Max-Planck-Institut für Festkörperforschung, Heisenbergstrasse 1, D-70569 Stuttgart, Germany

D. R. Noakes and C. E. Stronach
Department of Physics, Virginia State University, Petersburg, Virginia 23806

E. J. Ansaldo†
University of Saskatchewan, Saskatoon, Saskatchewan, Canada S7N 0W0
(Received 7 December 1998)

We have investigated the magnetic and the superconducting properties of the hybrid ruthenate-cuprate compound $RuSr_2GdCu_2O_8$ by means of zero-field muon-spin rotation (ZF-μSR) and dc magnetization measurements. The dc-magnetization data established that this material exhibits ferromagnetic order of the Ru moments [$\mu(Ru) \approx 1\ \mu_B$] below $T_C = 133$ K and becomes superconducting at a much lower temperature $T_c = 16$ K. The ZF-μSR experiments indicate that the ferromagnetic phase is homogeneous on a microscopic scale and accounts for most of the sample volume. They also suggest that the magnetic order is not significantly modified at the onset of superconductivity. [S0163-1829(99)07321-X]

I. INTRODUCTION

Since the discovery of superconductivity in the cuprate system $La_{2-x}Ba_xCuO_4$ in 1986,[1] an ever growing variety of high-T_c superconducting cuprate compounds has been synthesized all of which contain CuO_2 planes (some also contain CuO chains) as their essential structural elements which host the superconducting charge carriers.[2] Between the CuO_2 planes are various kinds of layers, typically NaCl-type, which are insulating and act merely as a charge reservoir. To date, the ruthenate compound Sr_2RuO_4 is the only known layered perovskitelike system which becomes superconducting even though it does not contain any CuO_2 planes or CuO chains.[3] Despite its rather low transition temperature $T_c = 1.5$ K, the study of its electronic and magnetic properties has become a very rich and active field of research.[4] In parallel, the electronic and magnetic properties of the related ruthenate compounds, such as, for example, the $SrRuO_3$ system which is an itinerant $4d$-band ferromagnet with $T_C \approx 165$ K, have attracted a great deal of interest.[5]

Another potentially promising and exciting direction of research has been prompted by the circumstance that the RuO_2 layers share the same square-planar coordination and a rather similar bond length with their CuO_2 counterparts. A whole new family of hybrid ruthenate-cuprate compounds may therefore be constructed whose members consist of different sequences of alternating RuO_2 and CuO_2 layers. Recently, one such a hybrid ruthenate-cuprate compound, the 1212-type $RuSr_2GdCu_2O_8$ system comprising CuO_2 bilayers and RuO_2 monolayers, has been synthesized as a single-phase material.[6] A subsequent study of its electronic and magnetic properties has revealed that this material exhibits electronic ferromagnetic order at a rather high Curie temperature $T_C = 133-136$ K and becomes superconducting at a significantly lower critical temperature $T_c = 15-40$ K (depending on the condition of preparation and annealing).[6–8] The most surprising observation, however, is that the ferromagnetic order does not vanish when superconductivity sets in at T_c. Instead, it appears that the ferromagnetic state remains largely unchanged and coexists with superconductivity. This finding implies that the interaction between the superconducting and the ferromagnetic order parameters is very weak and it raises the question of whether both order parameters coexist on a truly microscopic scale. Since the early investigations of Ginzburg in 1957,[9] the prevailing view is that the coexistence of a superconducting- (with singlet Cooper pairs) and a ferromagnetic order parameter is not possible on a microscopic scale since the electromagnetic interaction and the exchange coupling lift the degeneracy of the spin-up and the spin-down partners of the Cooper pair and cause strong pair breaking. Indeed, merely based on magnetization and transport measurements one cannot exclude the possibility that the $RuSr_2GdCu_2O_8$ samples may be

spatially inhomogeneous with some domains exhibiting ferromagnetic order and others superconducting order.[6] We note that unambiguous evidence for the occurrence of bulk superconductivity in $RuSr_2GdCu_2O_8$ has recently been obtained from specific-heat measurements which reveal a sizeable jump at T_c of $\Delta\gamma \equiv C_p/T \approx 0.35$ mJ/g at K^2, characteristic of a strongly underdoped cuprate superconductor.[10] In the following we report on muon-spin rotation (μSR) measurements which establish that the ferromagnetic order is uniform and homogeneous even on a microscopic scale.

The μSR technique is ideally suited for such a purpose since it provides an extremely sensitive local magnetic probe and, furthermore, allows one to reliably obtain the volume fraction of the magnetically ordered phase.[11] Here we present the result of a zero-field muon-spin rotation (ZF-μSR) study of a $RuSr_2GdCu_2O_8$ sample with $T_c = 16$ K and $T_C = 133$ K which provides evidence that the magnetic order parameter is spatially homogeneous and accounts for most of the sample volume. Furthermore, the ZF-μSR data establish that the ferromagnetic order is hardly affected by the onset of superconductivity and persists to the lowest available temperature of the experiment $T = 2.2$ K. The ZF-μSR data can be complemented by dc-magnetization measurements which establish the presence of ferromagnetic order from the observation of a spontaneous magnetization at $T_C = 133$ K and of hysteretic isothermal magnetic behavior with a remanent magnetization. It is shown that the ferromagnetic ordering involves the Ru magnetic moments with $\mu(\mathrm{Ru}) \approx 1.05(5)\mu_B$, while the larger Gd moments with $\mu\,(\mathrm{Gd}^{3+}) \approx 7.4(1)\mu_B$ remain paramagnetic down to very low temperatures. In addition, the magnetization measurements indicate an almost complete diamagnetic shielding effect below T_c.

II. EXPERIMENT

A. Sample preparation and characterization

Polycrystalline samples of the 1212-type system $RuSr_2GaCu_2O_8$ have been synthesized as previously described[8] by solid-state reaction of RuO_2, $SrCO_3$, Gd_2O_3, and CuO powders. The mixture was first decomposed at 960 °C in air. It was then ground, milled, and die-pressed into pellets. The first sintering step took place in flowing nitrogen atmosphere at 1010 °C. This step results in the formation of a mixture of the precursor material Sr_2GdRuO_6 and Cu_2O and is directed towards minimizing the formation of $SrRuO_3$.[6] The material was then reground before it was reacted in flowing oxygen for 10 h at 1050 °C. This sintering step was repeated twice with intermediate grinding and milling. Each reaction step was carried out on a MgO single-crystal substrate to prevent reaction with the alumina crucible. Finally the samples were cooled slowly to room temperature in flowing oxygen. Following this procedure we have also made a Zn-substituted $RuSr_2GdCu_{1.94}Zn_{0.06}O_8$ sample and a Y↔Gd cosubstituted sample $RuSr_2Gd_{0.9}Y_{0.1}Cu_2O_8$. X-ray-diffraction (XRD) measurements indicate that all samples are single phase 1212-type material and give no indication for traces of the ferromagnetic phase $SrRuO_3$. Figure 1(b) displays a representative XRD spectrum of $RuSr_2GdCu_2O_8$, the plus signs show the raw data and the solid line shows the result of the Rietveld refinement. The related structure of $RuSr_2GdCu_2O_8$ is shown in Fig. 1(a).

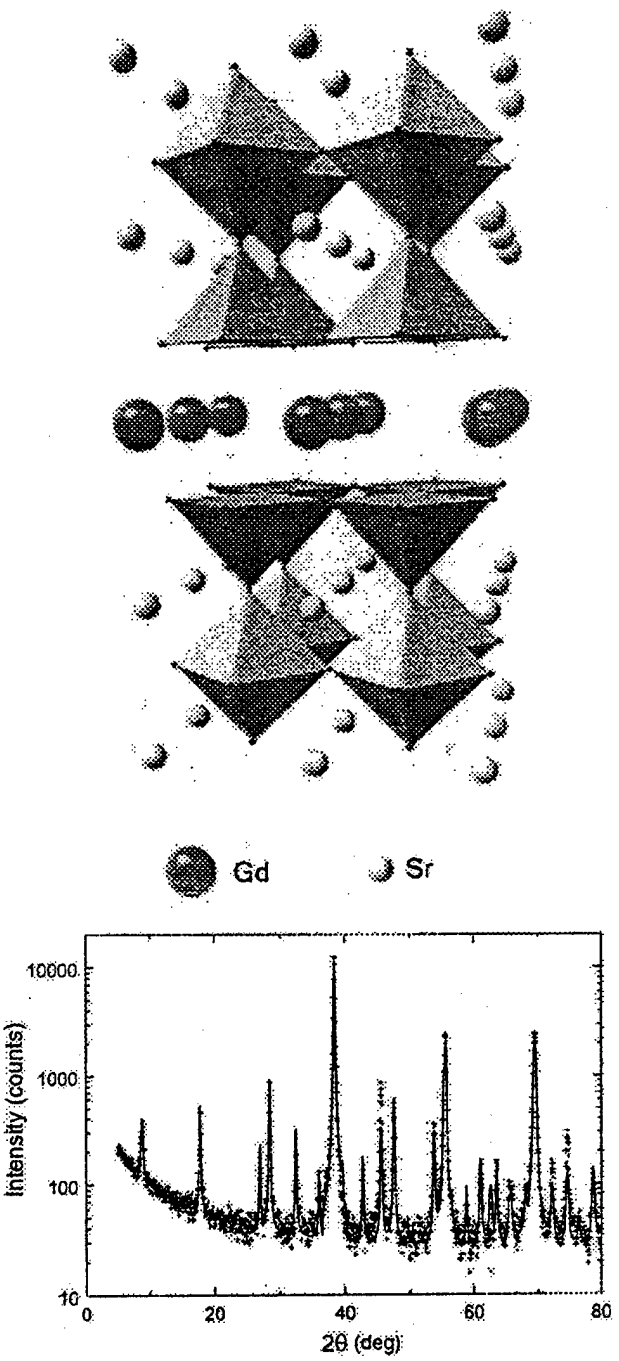

FIG. 1. (a) The structure of $RuSr_2GdCu_2O_8$ with the Cu atoms sited at the center of the base of the square pyramids and the Ru atoms at the center of the octahedra. (b) The x-ray-diffraction (XRD) spectrum for a $RuSr_2GdCu_2O_8$ sample (Co $K\,\alpha$ source). The plus signs (+) are the raw x-ray data and the solid line is the calculated Rietveld refinement profile for tetragonal (space group $P4/mmm$) $RuSr_2GdCu_2O_8$.

The electronic properties of $RuSr_2GdCu_2O_8$ have been characterized by measurements of the temperature-dependent resistivity and thermoelectric power. Representative results

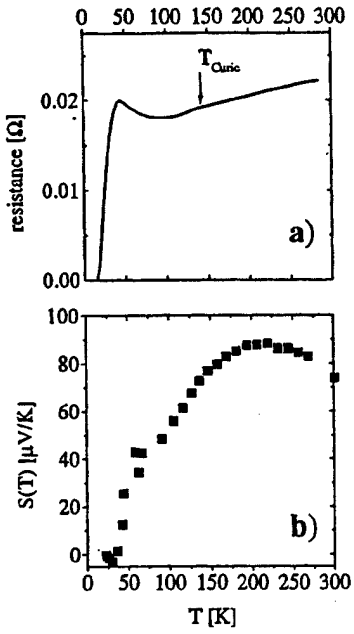

FIG. 2. (a) Temperature dependence of the resistivity ρ of $RuSr_2GdCu_2O_8$. (b) The temperature-dependent thermoelectric power $S(T)$.

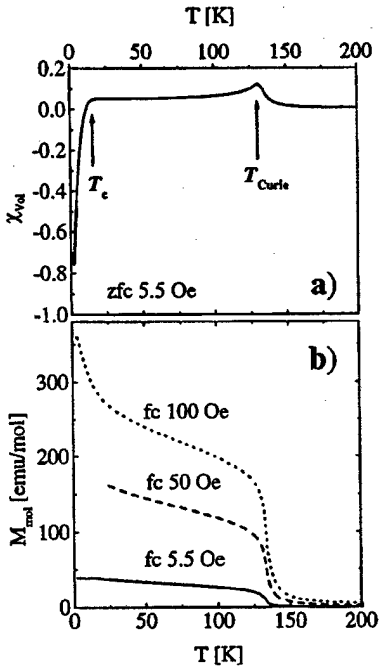

FIG. 3. (a) Temperature dependence of the zero-field-cooled dc volume magnetization χ_V of $RuSr_2GdCu_2O_8$. The arrows show the superconducting and the ferromagnetic transition at $T_c=16$ K and $T_C=133$ K, respectively. (b) The field-cooled molar magnetization M_{mol} for applied fields of $H=5.5$, 10, 100 Oe.

are shown in Figs. 2(a) and 2(b), respectively (see also Ref. 8). The temperature dependence of the thermoelectric power $S(T)$ and, in particular, its normal-state value of $S(300\ K)\approx 75\ \mu V/K$ is rather typical for a strongly underdoped cuprate superconductor with $T_c \ll T_{c,max}$, consistent with a hole content of $p\approx 0.07$ holes per CuO_2 planes and a value of $T_{c,max}$ of the order of 100 K.[8,12] The resistivity measurements indicate that the $RuSr_2GdCu_2O_8$ sample exhibits zero resistivity at a critical temperature of $T_c=16$ K. The precise value of T_c varies between 12 and 24 K, depending on synthesis conditions, and may be raised to 40 K by long-term annealing. The temperature dependence of the normal-state resistivity is again characteristic of a strongly underdoped superconducting cuprate compound. The ferromagnetic transition at $T_C=133$ K causes only a small yet noticeable drop in the resistivity indicating that the RuO_2 layer is almost insulating above T_C, while being poorly conducting in the ferromagnetic state.[5]

B. The technique of muon-spin rotation

The muon-spin rotation (μSR) experiments have been performed at the M15 beamline of TRIUMF in Vancouver, Canada, which provides 100% spin-polarized muons. The μSR technique is especially suited for the study of magnetic materials and allows one to study the homogeneity of the magnetic state on a microscopic scale and also to access its volume fraction.[11] The μSR technique typically covers a time window of 10^{-6}–10^{-9} s and allows one to detect internal magnetic fields over a wide range of 0.1 G to several Tesla. The 100% spin-polarized surface muons ($E_\mu \approx 4.2$ MeV) are implanted into the bulk of the sample where they thermalize very rapidly ($\sim 10^{-12}$ s) without any noticeable loss in their initial spin polarization. Each muon stops at a well-defined interstitial lattice site and, for the perovskite compounds, forms a muoxyl bond with one of the oxygen atoms.[13] The whole ensemble of muons is randomly distributed throughout a layer of 100–200 μm thickness and therefore probes a representative part of the sample volume. Each muon spin precesses in its local magnetic field B_μ with a precession frequency of, $\nu_\mu=(\gamma_\mu/2\pi)\cdot B_\mu$, where $\gamma_\mu/2\pi=135.5$ MHz/T is the gyromagnetic ratio of the positive muon. The muon decays with a mean lifetime of $\tau_{\mu^+}\approx 2.2\ \mu s^{-1}$ into two neutrinos and a positron which is preferentially emitted along the direction of the muon spin at the instant of decay. The time evolution of the spin polarization $P(t)$ of the muon ensemble can therefore be obtained via the time-resolved detection of the spatial asymmetry of the decay positron emission rate. More details regarding the zero-field (ZF) μSR technique are given below.

III. EXPERIMENTAL RESULTS

A. dc magnetization

Before we discuss the result of the μSR experiments, we first present some dc-magnetization data which establish that the $RuSr_2GdCu_2O_8$ sample exhibits a spontaneous magnetization at a ferromagnetic transition of $T_C=133$ K and becomes superconducting at a much lower temperature $T_c=16$ K. Figure 3(a) shows the temperature dependence of the volume susceptibility χ_V, which has been obtained after zero-field cooling the sample to $T=2$ K, then applying an external field of $H^{ext}=5.5$ Oe, and subsequently warming up to $T=200$ K. The density of the sample has been assumed to be $\rho=6.7$ g/cm^3 corresponding to stoichiometric $RuSr_2GdCu_2O_8$ with lattice parameters of $a=3.84$ Å and

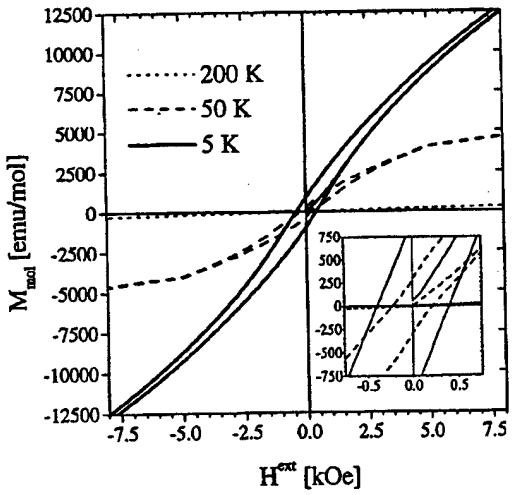

FIG. 4. The isothermal magnetization loops of $RuSr_2GdCu_2O_8$ at $T=5$, 50, and 200 K. The inset shows a magnification of the low-field region.

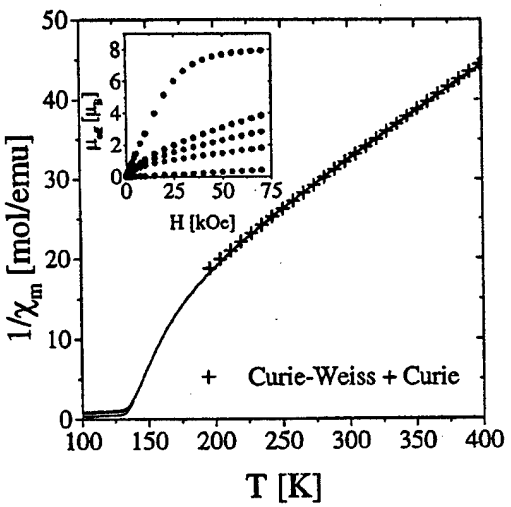

FIG. 5. The temperature-dependent inverse molar susceptibility $1/\chi_m$ for the high-temperature range of 400 K$>T>$100 K. The plus signs show the best fit using a two component Curie-Weiss + Curie function. Shown in the inset is the saturation magnetization in units of effective Bohr magnetons per unit volume as a function of applied field at temperatures of $T=2$, 30, 50, 100, 200 K.

$c=11.57$ Å.[8] The superconducting transition is evident in Fig. 3(a) from the onset of a pronounced diamagnetic shift below $T_c=16$ K. The diamagnetic shift at the lowest available temperature of $T=2$ K corresponds to an almost complete diamagnetic shielding of the sample volume, implying that at least the surface region of the sample is homogeneously superconducting. In fact, all pieces that have been cut from the pellet exhibit a similarly large diamagnetic shielding effect (small differences can be attributed to different demagnetization factors). Nevertheless, the dc-magnetization measurements cannot give unambiguous evidence for the presence of bulk superconductivity since an almost complete diamagnetic shielding may also be caused by a filamentary structure of superconducting material in a small fraction of the otherwise nonsuperconducting material. We note however, that unequivocal evidence for the occurrence of bulk superconductivity in $RuSr_2GdCu_2O_8$ has recently been obtained from specific-heat measurements which reveal a sizeable jump of $\Delta\gamma \equiv C_p/T \approx 0.35$ mJ/g at K^2 at T_c, comparable to or greater than that seen in other underdoped cuprates.[10] For comparison in strongly underdoped $YBa_2Cu_3O_{7-\delta}$ it is found that $\Delta\gamma \approx 0.2-0.3$ mJ/g at K^2.[2,14] We also note that the specific-heat measurements have been performed on the same samples which have been studied by μSR- and dc-magnetization measurements. Figure 3(b) displays the (low) field-cooled molar magnetization M_m for applied fields of $H^{ext}=5.5$, 50, and 100 Oe. The ferromagnetic transition at $T_C=133$ K is evident from the sudden onset of a spontaneous magnetization. Evidently, the magnetic order parameter has at least a sizeable ferromagnetic component and it persists almost unchanged to the lowest measured temperature $T=2$ K. In particular, it does not appear to weaken as superconductivity sets in at $T_c=16$K. Additional evidence for the presence of ferromagnetic order is presented in Fig. 4, which shows that the isothermal magnetization loops at $T=5$ and 50 K exhibit hysteretic magnetic behavior with a remanent magnetization $M_{rem} \approx 400$ Oe at 5 K and 200 Oe at 50 K.

Having established the existence of ferromagnetic order, the question arises of whether it involves the Ru moments or the Gd moments. In the following we present high-temperature susceptibility data which indicate that the ferromagnetic order involves only the Ru moments, whereas the Gd moments remain in the paramagnetic state below T_C. Figure 5 shows the inverse molar susceptibility, $1/\chi_m \approx (M_m/H^{ext})^{-1}$ obtained for different external fields in the range $5.5 \leq H^{ext} \leq 1000$ Oe (solid lines) in the temperature region 200 K$<T<$400 K. Shown by the plus signs (+) is the best fit to the experimental data using a two-component Curie-Weiss+Curie function, $\chi = C_1/(T-\Theta)+C_2/T$, with $\Theta = T_C = 133$ K kept fixed. This function describes the experimental data rather well and it gives us very reasonable values for the magnetic moments, with $\mu_1 = 1.05(5)\mu_B$ for the moments that order at T_C and $\mu_2 = 7.4(1)\mu_B$ for the moments that remain paramagnetic below T_C. The magnetic moment of the paramagnetic component agrees reasonably well with the expected magnetic moment of Gd^{3+} which for a free Gd^{3+} ion[15] is $\mu(Gd^{3+}) = 7.94\mu_B$ and $\mu(Gd^{3+}) = 7.4\mu_B$ for the structurally similar $GdBa_2Cu_3O_{7-\delta}$ compound.[16] On the other hand, the value of the Ru moments with $\mu(Ru) = 1.05(5)\mu_B$ also appears to be reasonable. For Ru^{5+} the number of $4d$ electrons is 3 and the free-ion value of the magnetic moment is $3\mu_B$ for the high-spin state and $1\mu_B$ for the low-spin state. The experimentally observed value of $\mu(Ru) = 1.05(5)\mu_B$ therefore seems to imply that Ru^{5+} is in the low-spin state. Shown in the inset of Fig. 5 is the field-dependent magnetization for the temperatures $T=2$, 30, 50, 100, and 300 K. The low-temperature magnetization can be seen to saturate at a value of $\mu_{sat} \approx 8\mu_B$, as may be expected for a system that contains one Gd moment per formula unit with $\mu(Gd) = 7\mu_B$ plus one Ru moment with $\mu(Ru) = 1\mu_B$.

The idea that the Gd moments do not participate in the ferromagnetic transition at $T_C=133$ K is supported by the result of dc-magnetization measurements on the 10% Y↔Gd cosubstituted $RuSr_2Gd_{0.9}Y_{0.1}Cu_2O_8$. Figures 6(a) and 6(b)

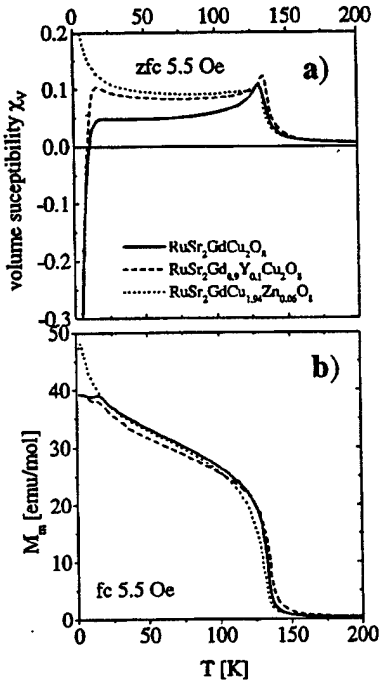

FIG. 6. (a) The temperature-dependent volume susceptibility χ_V of $RuSr_2GdCu_2O_8$ (solid line), for Zn-substituted $RuSr_2GdCu_{1.94}Zn_{0.06}O_8$ (dotted line) and for Y↔Gd cosubstituted $RuSr_2Gd_{0.9}Y_{0.1}Cu_2O_8$ (dashed line). (b) The temperature-dependent molar magnetization M_m, shown by the same symbols as in (a).

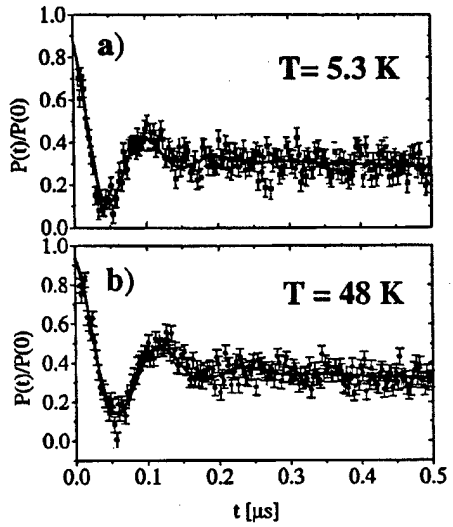

FIG. 7. The time-resolved normalized muon-spin polarization, $P(t)/P(t=0)$, at temperatures of (a) $T=5.3$ K$<T_c$ and (b) $T_c<T=48$ K$<T_C=133$ K. The large oscillatory component gives clear evidence for the presence of a magnetically ordered state.

display the zero-field-cooled,- and the field-cooled susceptibilities (dashed lines) and compare them with the corresponding data on the pure $RuSr_2GdCu_2O_8$ sample (solid line). It is evident that the ferromagnetic transition is not significantly affected by the partial substitution of nonmagnetic Y^{3+} for magnetic Gd^{3+}. Also shown in Figs. 6(a) and 6(b) by the dotted lines are the results for the Zn-substituted $RuSr_2Cu_{1.94}Zn_{0.06}O_8$ sample. The circumstance that the ferromagnetic order is not affected by the Zn substitution supports our view that the majority of the Zn impurities has been introduced into the CuO_2 layers while hardly any of them reside within the RuO_2 layers. Moreover, we infer from the rapid T_c suppression upon Zn substitution that only the CuO_2 layers host the superconducting charge carrier in $RuSr_2GdCu_2O_8$.

B. Zero-field muon-spin-rotation (ZF-μSR)

Next we discuss the result of the zero-field (ZF) μSR experiments. Figures 7(a) and 7(b) show representative ZF-μSR spectra for the evolution of the normalized time-resolved muon-spin polarization $P(t)/P(0)$ at temperatures of $T=5$ and 48 K. The value of the initial muon-spin polarization $P(0)$ has been determined by a transverse field (TF) μSR experiment performed on the same sample at a temperature above T_C. In the ferromagnetic state below $T_C=133$ K we find that the spectra are well described by the relaxation function:

$$P(t)/P(t=0)=A_1\exp(-\lambda t)\cos(2\pi\langle\nu_\mu\rangle t)+A_2\exp(-\Lambda t), \quad (1)$$

where $\langle\nu_\mu\rangle$ is the average muon-spin precession frequency which corresponds to the average value of the spontaneous internal magnetic field at the muons sites, $\langle\nu_\mu\rangle=\gamma_\mu/2\pi\langle B_\mu\rangle$, with $\gamma_\mu=835.4$ MHz/T being the gyromagnetic ratio. The damping rate of the nonoscillating (longitudinal) component Λ is proportional to the dynamic spin-lattice relaxation rate $\Lambda\sim 1/T_1$, whereas the relaxation rate of the oscillating (transverse) component, λ is dominated by the static distribution of the local magnetic field, i.e., $\lambda\approx\gamma_\mu\langle\Delta B_\mu\rangle$. Figure 8 shows the temperature dependence of (a) the precession frequency $\langle\nu_\mu\rangle(T)$, (b) the transverse relaxation rate $\lambda(T)$, and (c) the longitudinal relaxation rate $\Lambda(T)$.

Before we discuss the ZF-μSR data in more detail, we first emphasize the most important implications, which are evident from Figs. 7 and 8. Firstly, the presence of an oscillating component in the ZF-μSR spectra for $T<T_C=133$ K gives unambiguous evidence for an ordered magnetic state which is homogeneous on a microscope length scale (of typically 20 Å). Secondly, from the amplitude of the oscillating component ($A_1\approx 2/3$) we can deduce that the magnetically ordered state accounts for more or less the entire volume of the sample. And thirdly, from the temperature dependence of the μSR signal it becomes clear that the magnetic order persists almost unchanged in the superconducting state.

1. The volume fraction of the magnetic phase

In the following we outline how the volume fraction of the magnetically ordered phase is obtained from the amplitude of the oscillating component of the ZF-μSR spectra. For a polycrystalline sample with randomly orientated grains in zero external field the local magnetic field, on average, is parallel (perpendicular) to the direction of the muon-spin direction with probability 1/3 (2/3). For a homogeneous magnetically ordered sample, one therefore expects that 2/3 of the amplitude of the ZF-μSR signal (the transverse compo-

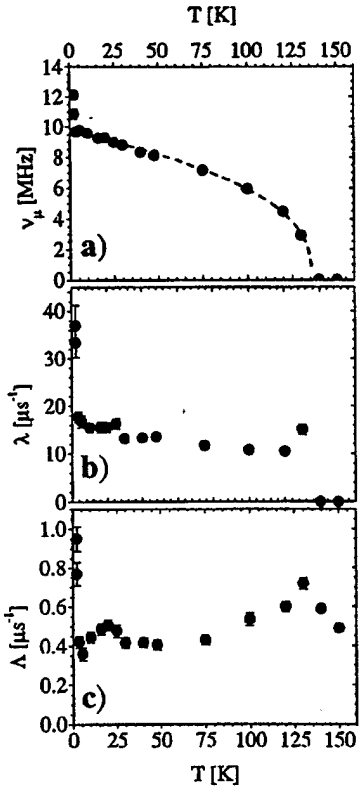

FIG. 8. The temperature dependence of the μSR signal of $RuSr_2GdCu_2O_8$. (a) The muon-spin precession frequency, $\nu_\mu(T)$ (MHz)=135.5 (MHz/T) $\langle B_\mu \rangle$. Shown by the dashed line is the best fit using the scaling function $\nu_\mu(T)=\nu_0(1-T/T_C)^\beta$, with $\beta=0.333(5)$, $T_C=133(1)$ K, and $\nu_0=9.70(5)$ MHz [$B_\mu=720(1)$G]. (b) The relaxation rate of the precessing component, $\lambda(T)$. (c) The relaxation rate of the nonprecessing component, $\Lambda(T)\sim 1/T_1$.

nent) exhibit an oscillatory behavior, while 1/3 of the signal (the longitudinal component) is nonoscillating and is only slowly damped due to spin-flip excitations. On the other hand, for a sample with inhomogeneous magnetic order, for example containing nonmagnetic regions, the amplitude of the oscillating signal will be accordingly reduced and a second nonoscillating transverse component will appear. If the nonmagnetic regions are microscopically small, this nonoscillating component is likely to have a rather large damping rate of the order of $\lambda\sim\gamma_\mu\langle B_\mu\rangle$ due to stray fields which are imposed by the neighboring magnetic domains. From Figs. 7(a) and 7(b) it can be seen that the ZF-μSR data on $RuSr_2GdCu_2O_8$ give no indication for such an inhomogeneous magnetic state. As was mentioned above, the amplitude of the initial muon-spin polarization $P(t=0)$ has been determined from a transverse-field (TF)-μSR measurement. From the size of the amplitude of the oscillatory component we deduce that more than 80% of the sample is magnetically ordered below $T_C=133$ K. Based on this analysis we estimate that the volume fraction of any disordered magnetic or nonmagnetic phase must be well below 20%. Note that some of the muons (typically 10–20%) do not stop inside the sample but somewhere in the cryostate walls. In the ZF-μSR experiment these muons give rise to a missing fraction since their spin-polarization is much more slowly damped than for the rest of the signal. In the TF-μSR experiment, however, this very slowly damped component can be detected via its precession in the external field and it contributes to the total muon-spin polarization $P(0)$. The 80% fraction of the magnetically ordered phase therefore has to be regarded as a lower bound. In fact, it is rather likely that the entire sample volume is magnetically ordered. Finally, we note that the muons apparently occupy only one muon site, since only one precession frequency is seen in the ZF-μSR spectra. Also it is clear from the ZF-μSR data that muon diffusion effects are negligibly small below $T_C=133$ K, similar to the other cuprate superconductors where muon diffusion is observed only at significantly higher temperatures of $T\geqslant 250$ K.[13]

2. Local magnetic field at the muon site

It is evident from Fig. 8(a) that the muon-spin precession frequency (the local field at the muon site) does not exhibit any strong anomaly at the superconducting transition temperature T_c. Instead, as shown by the dashed line, the temperature dependence of the muon-spin precession frequency $\langle\nu_\mu\rangle(T)$ (and thus of the magnetic order parameter) is well described by the function $\nu_\mu(T)=\nu_0(1-T/T_c)^\beta$, with $\nu_0=9.7(1)$ MHz [corresponding to $\langle B_\mu\rangle(T\rightarrow 0)\approx 720(10)$G], $T_c=133(1)$ K, and $\beta=0.333(5)$. This functional form is strictly valid only in the critical regime close to T_C but it can be seen to provide a reasonable description of the magnetic order parameter over a fairly wide temperature range of $T_C\geqslant T\geqslant 5$ K. The anomaly at very low temperature arises most likely from the magnetic ordering transition of the Gd moments at $T_N\approx 2.6$ K. Note that for the structurally related compound $GdBa_2Cu_3O_{7-\delta}$ (Gd-123) the antiferromagnetic ordering transition of the Gd moment occurs at a very similar temperature of $T_N=2.3$ K.[16,17] The value of the critical exponent $\beta=0.333$ is close to the theoretical value 0.345 in the 3D *XY* model.[18] We cannot determine with certainty the number of components in the spin system with these data and, in particular, distinguish between the two-component *XY* ($\beta=0.345$) and the three-component Heisenberg ($\beta=0.365$) models. The contribution of ferromagnetic fluctuations above T_C to the susceptibility provides better discrimination as will be discussed later.

The oscillating transverse component exhibits a damping rate of the order of $\lambda\approx 10$–$15\ \mu s^{-1}$ corresponding to a spread in the local magnetic field of $\langle\Delta B_\mu\rangle/\langle B_\mu\rangle\approx 0.2$. This 20% spread of the local magnetic field does not seem to agree with a scenario where the ferromagnetic order is assumed to exhibit a spiral modulation (with a wavelength shorter than the superconducting coherence length of typically 20 Å in the cuprates) and/or to be spatially inhomogeneous as in $ErRh_4B_4$,[19] $HoMo_6S_8$,[20] and Y_9Co_7.[21] Instead, we emphasize that the observed spread in the local magnetic field can be accounted for by the grain-boundary effects and by the differences in the demagnetization factors of the individual grains which naturally arise for a polycrystalline sample that has a very small average grain size of about 1 μm.[8] Also, we point out that recent transmission-electron-microscopy studies have revealed that our present Ru-1212 sample contains [100] rotation twins and also exhibits some cationic disorder due to the intermixing of Sr↔Gd and to a lesser extent of Ru↔Cu.[8] These kinds of structural imperfections certainly tend to further increase the transverse relaxation rate λ of the

ZF-μSR spectra. Meanwhile, we have prepared Ru-1212 samples which are structurally more perfect (by sintering at slightly higher temperature and for longer periods).[8] Recent dc-magnetization measurements have shown that these crystallographic defects do not affect the fundamental magnetic and superconducting behavior. In fact, both the superconducting and the ferromagnetic transitions become somewhat sharper and T_c and T_C are slightly increased for these structurally more perfect samples.[8] Additional μSR measurements on these samples are presently under way.

3. Longitudinal relaxation rate, $\Lambda \sim 1/T_1$

The temperature dependence of the relaxation rate of the nonoscillating component of the ZF-μSR signal, $\Lambda(T) \sim 1/T$, is shown in Fig. 8(c). As a function of decreasing temperature $\Lambda(T)$ can be seen to exhibit a cusplike feature at the ferromagnetic transition of the Ru moments at $T_C = 133$ K and a steplike increase at very low temperature which most likely is related to the ordering of the Gd moments. The cusp feature at $T_C = 133$ K characterizes the slowing down of the spin dynamics of the Ru moments as the ferromagnetic transition is approached. The cusp maximum occurs when the spin-fluctuation rate τ_c equals the typical μSR time scale for $\tau_c \sim 10^{-6}$.[11] Note, that in the ferromagnetically ordered state that longitudinal relaxation rate remains unusually large with values of $\Lambda(T \ll T_C) \approx 0.3-0.4\ \mu s^{-1}$ that are at least an order of magnitude larger than expected for a classical ferromagnet[22] (where two-magnon excitations provide the major contribution to spin dynamics). We have confirmed by a μSR measurements in a longitudinal field of $H^{LF} = 6$ kOe that this large relaxation rate is indeed characteristic for the longitudinal component of the μSR signal. At present we cannot provide a definite explanation of the origin of the unusually large value of Λ. However, we emphasize that the $RuSr_2GdCu_2O_8$ system can be expected to exhibit a rather complex magnetic behavior since, besides the ferromagnetically ordered Ru moments, it also contains the larger Gd moments with $\mu(Gd^{3+}) \approx 7.4 \mu_B$ which remain paramagnetic below T_C. The magnetic ordering transition of the Gd moments at $T \approx 2.6$ K is evident in the ZF-μSR data in Figs. 8(a)–8(c) from the sudden increase in the local magnetic field (or the μSR precession frequency, $\langle \nu_\mu \rangle$) and a corresponding increase in both relaxation rates, λ and Λ. In addition, we note that recently it has been shown by μSR measurements that in strongly underdoped high-$T_c$cuprate superconductors (like the present $RuSr_2GdCu_2O_8$ compound) also the Cu moments exhibit a spin-glass-type freezing transition at low temperature.[23] Finally, it appears that the longitudinal relaxation rate Λ exhibits an additional weak anomaly at a temperature of $T \approx 20$ K, i.e., in the vicinity of the superconducting transition at $T_c = 16$ K. At present we are not sure whether this effect is related to the onset of superconductivity. From Fig. 8(b) it appears that the transverse relaxation rate also exhibits a steplike increase in the same temperature range. The local magnetic field at the muon site, however, [see Fig. 8(a)] does not seem to exhibit any anomaly in the vicinity of T_c. We expect that further μSR measurements on rare-earth substituted $RuSr_2Gd_{1-x}R_xCu_2O_8$ samples, as well as on less strongly underdoped samples with higher critical temperatures of T_c up to 40 K, should shed more light on the complex magnetic behavior and its interplay with superconductivity in the Ru-1212 system.

TABLE I. The local magnetic field at the muon site $\langle B_\mu \rangle$, obtained from the dipolar-field calculation. The results are shown for two different muon sites and for three different orientations with the Ru moments [$\mu(Ru^{5+}) = 1 \mu_B$] ferromagnetically ordered along the Ru-O bond [100], along the diagonal [110], or perpendicular to the RuO_2 planes [001]. Note that for the [110] orientation there exist two magnetically inequivalent muon sites.

Muon site	[100]	[110]	[001]
(0.13,0.225,0.16)	960 G	1068/805 G	1471 G
(0.128,0.222,0.175)	740 G	824/665 G	1231 G

C. Dipolar field calculation

While the ZF-μSR data give clear evidence for the presence of a homogeneous magnetically ordered state, they do not provide any direct information about the origin of the magnetic moments, the type of the magnetic order, and its direction. Based on dipolar-field calculations of the local magnetic field at the muon site, however, one can test the consistency with an assumed magnetic structure. The result of these calculations depends on the location of the interstitial muon site and also on the orientation of the Ru moments. Unfortunately, for the Ru-1212 system neither of these is accurately known at present. Nevertheless, it seems plausible that the muon site is similar to that in $YBa_2Cu_3O_{7-\delta}$ (and other related cuprate compounds) where the positive muon forms a hydroxyl bond with the apex oxygen and is located at the so-called "apical site" near the point $(0.12a, 0.225b, 0.14c)$.[13] Indeed, as is summarized in Table I, we obtain rather good agreement with the experimental value of $\langle B_\mu \rangle (T \to 0) = 720$ G if we take a similar apical site near the point $(0.13a,\ 0.22b,\ 0.16-0.17c)$ and assume that the ferromagnetically ordered Ru moments [$\mu(Ru) = 1 \mu_B$]are oriented along the RuO_2 plane either along the Ru-O bond, [100], or along the diagonal [110] (see Table I). For the [110] orientation, however, there exist two magnetically inequivalent muon sites which should give rise to two distinctive precession frequencies in the μSR spectra (which are not observed experimentally). For the Ru moments oriented perpendicular to the RuO_2 layer along [001] the resulting local magnetic field at the apex site is significantly larger than the experimental value. In order to obtain reasonable agreement with experiment for the [001] orientation, one has to assume that the muon site is located much closer to the CuO_2 planes. Such a muon site, however, is not very realistic (simply speaking the positive muon is repelled by the positively charged CuO_2 planes) and has not been observed in any of the related cuprate compounds. We thus tentatively conclude that the moments align in-plane consistent with the two-component XY scenario. While this result is rather convenient in terms of the coexistence of the ferromagnetic order of the Ru moments and the superconductivity which resides within the CuO_2 layers as discussed below, one has to keep in mind that the underlying assumptions are rather crude. For more detailed and decisive information on the structure and

the orientation of the Ru spin order we must await the result of neutron-scattering experiments.

IV. A POSSIBLE SCENARIO FOR COEXISTENCE OF FERROMAGNETIC AND SUPERCONDUCTING ORDER

Having established that the ferromagnetic and the superconducting order parameter coexist on a microscopic scale, we arrive at the important question as to how this system manages to avoid strong pair-breaking effects. We suspect that the answer is closely related to the layered structure of the hybrid ruthenate-cuprate compound and, in particular, to the purely two-dimensional coherent charge transport in the strongly underdoped CuO_2 planes. We envisage a scenario where the ferromagnetically ordered Ru spins are aligned in the RuO_2 plane having a very large out-of-plane anisotropy while the charge dynamics of the superconducting CuO_2 planes is purely two-dimensional, i.e., coherent charge transport occurs only along the direction of the CuO_2 planes. For such a configuration the principal pair-breaking effect due to the electromagnetic interaction can be minimized, since the dot product of the magnetic vector potential (which then is normal to the planes) and the momentum of the Cooper pair (which is parallel to the planes) vanishes. An additional requirement is that the direct hyperfine interaction between the superconducting electrons of the CuO_2 planes and the ordered Ru spins has to be extremely small. Both requirements may be fulfilled in the present Ru-1212 system due to the confinement of the superconducting electrons of the strongly underdoped CuO_2 planes. The absence of magnetic pair breaking is suggested by the fact that the T_c value is fully consistent with the underdoped state indicated by the thermoelectric power.[12] So far we have been unable to significantly increase the doping state (by, e.g., Ca substitution) so as to explore these implications. Furthermore, we have not yet succeeded in crystallographically aligning powders or growing single crystals which would allow one to investigate the magnetic anisotropy. However, further information can be obtained by examining the ferromagnetic fluctuations above T_C as seen in the divergence of the susceptibility. Figure 9 shows d_χ/dT plotted versus (T/T_C-1) for the zero-field-cooled susceptibility for $T>T_C$. The slope of $-2.30(3)$ indicates a critical exponent of $\gamma=1.30(3)$ consistent with 3D *XY* fluctuations for which $\gamma=1.32$ (Ref. 18) and again consistent with orientation of the Ru moments within the *a-b* plane.

Finally, we note that an alternative (and highly speculative) explanation for the coexistence of high-T_c superconductivity and ferromagnetic order in the present Ru 1212 superconductor could be that the superconducting order parameter has a nonzero angular momentum which itself breaks time-reversal symmetry. Such an unconventional order parameter symmetry has been discussed also in the context of the Sr_2RuO_4 superconductor. We point out, however, that at present we have no evidence in favor of such a scenario.

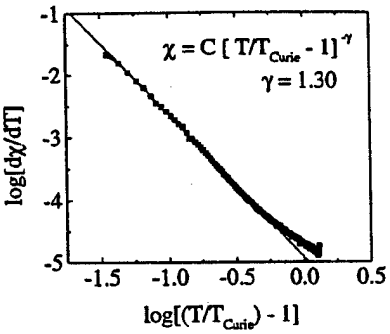

FIG. 9. d_χ/dT plotted versus (T/T_C-1) for the zero-field-cooled susceptibility in the temperature range of $T>T_C$. The slope of $-2.30(3)$ indicates a critical exponent of $\gamma=1.30(3)$ consistent with 3D *XY* fluctuations for which $\gamma=1.32$ (Ref. 18) and consistent with orientation of the Ru moments within the *a-b* plane.

V. CONCLUSIONS

In summary, we have performed dc-magnetization and zero-field muon-spin rotation (ZF-μSR) measurements which characterize the superconducting and the magnetic properties of the hybrid cuprate-ruthenate compound $RuSr_2GdCu_2O_8$. The dc-magnetization data establish that this material exhibits ferromagnetic order (or at least magnetic order with a sizeable ferromagnetic component) below $T_C=133$ K and becomes superconducting at a much lower temperature of $T_c=16$ K. We obtain evidence that superconducting charge carriers originate from the CuO_2 planes, while the ferromagnetic order is associated with the Ru moments with $\mu(\mathrm{Ru})\approx 1\,\mu_B$. The larger Gd moments with $\mu(\mathrm{Gd})\approx 7.4\,\mu_B$ do not appear to participate in the ferromagnetic transition but remain paramagnetic to very low temperature and undergo most likely an antiferromagnetic transition at $T_N=2.6$ K. The ZF-μSR experiments provide evidence that the ferromagnetic phase is homogeneous on a microscope scale and accounts for most of the sample volume. Furthermore, they indicate that the magnetically ordered state is not significantly modified by the onset of superconductivity. This rather surprising result raises the question as to how ferromagnetic and superconducting order can coexist on a microscopic scale while avoiding strong pair-breaking effects that tend to destroy superconductivity. We have outlined a possible scenario which relies on the two-dimensional charge dynamics of the CuO_2 planes and the assumption that the ferromagnetic order parameter of the Ru moments is confined to the RuO_2 layers.

ACKNOWLEDGMENTS

We would like to acknowledge S. Kreitzman and B. Hitti for the technical support during the μSR experiments at TRIUMF. J.L.T. thanks the Royal Society of New Zealand for financial support. Ch.N. and Th.B. thank the German BMBF for financial support. C.E.S. and D.R.N. were supported by U.S. Air Force Office of Scientific Research Grant No. F49620-97-1-0297.

*Permanent address: Institute of Experimental Physics, Warsaw University, Hoża 69, 00-681 Warsaw, Poland.
†Present address: 1318 Tenth St., Sakatoon, Saskatchewan, Canada S7H OJ3.

[1] J. G. Bednorz and K. A. Müller, Z. Phys. B **64**, 189 (1986).
[2] R. J. Cava, Science **247**, 656 (1990).
[3] Y. Maeno, H. Hashimoto, K. Yoshida, S. Nishizaki, T. Fujita, J. G. Bednorz, and F. Lichtenberg, Nature (London) **372**, 532 (1994).
[4] See, for example, Y. Maeno, S. Nishizaki, K. Yoshida, S. Ikeda, and T. Fujita, J. Low Temp. Phys. **105**, 1577 (1996).
[5] See, for example, L. Klein, J. S. Dodge, C. H. Ahn, J. W. Reiner, L. Mieville, T. H. Geballe, M. R. Beasley, and A. Kapitulnik, J. Phys.: Condens. Matter **8**, 10 111 (1996); G. Cao, S. McCall, M. Shepard, J. E. Crow, and R. P. Guertin, Phys. Rev. B **56**, 321 (1997); I. I. Mazin and D. J. Singh, Phys. Rev. B **56**, 2556 (1997).
[6] L. Bauernfeind, W. Widder, and H. F. Braun, Physica C **254**, 151 (1995); L. Bauernfeind, W. Widder, and H. F. Braun, J. Low Temp. Phys. **105**, 1605 (1996); L. Bauernfeind, W. Widder, and H. F. Braun, in *Proceedings of the Fourth Euro Ceramics*, edited by A. Barone, D. Fiorani, and A. Tampieri (Gruppo Editorale Faenza Editrice, Italy, 1995), Vol. 6, p. 329.
[7] I. Felner, U. Asaf, Y. Levi, and O. Millo, Phys. Rev. B **55**, R3374 (1997).
[8] J. L. Tallon, C. Bernhard, M. E. Bowden, T. M. Stoto, B. Walker, P. W. Gilbert, G. V. M. Williams, D. M. Pooke, and M. R. Presland (unpublished).
[9] V. L. Ginsburg, Sov. Phys. JETP **4**, 153 (1957).
[10] J. L. Tallon, J. W. Loram, G. V. M. Williams, and C. Bernhard (unpublished).
[11] See, for example, A. Schenck, *Muon Spin Rotation: Principles and Applications in Solid State Physics* (Adam Hilger, Bristol, 1986).
[12] S. D. Obertelli, J. R. Cooper, and J. L. Tallon, Phys. Rev. B **46**, 14 928 (1992).
[13] M. Weber, P. Birrer, F. N. Gygax, B. Hitti, E. Lippelt, H. Maletta, and A. Schenck, Hyperfine Interact. **63**, 207 (1990); N. Nishida and H. Miyatake *ibid.* **63**, 183 (1990).
[14] J. W. Loram, K. A. Mirza, J. R. Cooper, and W. Y. Liang, Phys. Rev. Lett. **71**, 1740 (1993).
[15] N. W. Ashcroft and N. D. Mermin, *Solid State Physics* (Holt, Rinehart, and Winston, Philadelphia, 1976).
[16] J. O. Willis, Z. Fisk, J. D. Thompson, S.-W. Cheong, R. A. Aiken, J. L. Smith, and E. Zirngiebl, J. Magn. Magn. Mater. **67**, L139 (1987); D. McK. Paul, H. A. Mook, A. W. Hewat, B. C. Sales, L. A. Boatner, R. J. Thompson, and M. Mostoller, Phys. Rev. B **37**, 2341 (1988).
[17] See, for example, A. Golnik, Ch. Niedermayer, E. Recknagel, M. Rossmanith, A. Weidinger, J. I. Budnick, B. Chamberland, M. Filipkowsky, Y. Zhang, D. P. Yang, L. L. Lynds, F. A. Otter, and C. Baines, Phys. Lett. A **125**, 71 (1987); Ch. Niedermayer, H. Glückler, A. Golnik, U. Binninger, M. Rauer, E. Recknagel, J. I. Budnick, and A. Weidinger, Phys. Rev. B **47**, 3427 (1993).
[18] J. C. Le Guillou and J. Zinn-Justin, Phys. Rev. B **21**, 3976 (1980).
[19] W. A. Fertig, D. C. Johnston, L. E. DeLong, R. W. McCallum, M. B. Maple, and B. T. Mattias, Phys. Rev. Lett. **38**, 987 (1977); D. E. Moncton, D. B. McWhan, P. H. Schmidt, G. Shirane, W. Thomlinson, M. B. Maple, H. B. MacKay, L. D. Woolf, Z. Fisk, and D. C. Johnston, *ibid.* **45**, 2060 (1980).
[20] M. Ishikawa and O. Fischer, Solid State Commun. **23**, 37 (1977); P. Burlet, J. Flouquet, J. L. Genicon, R. Horyn, O. Pena, and M. Sergent, Physica C **215**, 127 (1995); J. W. Lynn, G. Shirane, W. Thomlinson, R. N. Shelton, and D. E. Moncton, Phys. Rev. B **24**, 3817 (1981).
[21] B. V. Sarkissian, J. Appl. Phys. **53**, 8070 (1982); E. J. Ansaldo, D. R. Noakes, J. H. Brewer, R. Keitel, D. R. Harshman, M. Semba, C. Y. Huang, and B. V. B. Sarkissian, Solid State Commun. **55**, 193 (1985).
[22] See, for example, A. Yaouanc and P. Dalmas de Reotier, J. Phys.: Condens. Matter **3**, 6195 (1991); P. C. M. Gubbens *et al.*, Hyperfine Interact. **85**, 239 (1994).
[23] See, for example, Ch. Niedermayer, C. Bernhard, T. Blasius, A. Golnik, A. Moodenbaugh, and J. I. Budnick, Phys. Rev. Lett. **80**, 3843 (1998).

J. Phys.: Condens. Matter 11 (1999) 1589–1600. Printed in the UK PII: S0953-8984(99)98109-2

A correlation length measured by zero-field muon spin relaxation in disordered magnets

D R Noakes
Physics Department, Virginia State University, Petersburg, VA 23806, USA

Received 5 October 1998, in final form 2 December 1998

Abstract. Muon spin relaxation, as a local magnetic probe, is not normally expected to be able to provide measurements of any magnetic correlation length. When anomalously shallow static zero-field muon spin relaxation functions were observed for $CeNi_{1-x}Cu_xSn$ and a small number of other highly disordered magnetic systems, however, and a 'Gaussian-broadened Gaussian' relaxation function shown to fit them, it was suggested that an unusual short-range correlation among local moments in the material was acting. 'Range-correlated moment magnitude variation', in which ion-moment orientations are completely random, but moment magnitude varies slowly from place to place, is shown by Monte Carlo numerical simulation on a lattice of moments to generate the qualitative form of shallow static zero-field relaxation observed. Thus, the *shape* of the zero-field muon spin relaxation function is sensitive to a correlation length.

1. Introduction

Positive-muon spin relaxation (μSR) is a probe of local magnetic fields in materials (for introductory reviews, see [1]) that is particularly useful when carried out in zero external field (ZF). The magnetic moment of a μ^+ stopped at an interstitial site in a solid precesses in the local field at that site, and then emits a positron preferentially in the direction of the μ^+-moment at the instant of decay. Knowing the initial polarization of the muons and detecting the directions of the decay positrons, the experimenter can measure the time evolution of the polarization in the direction of initial orientation, called the (longitudinal) 'muon spin relaxation function', $G_z(t)$. In ferromagnetic or antiferromagnetic states, the well-ordered array of ion moments will often generate a unique field at the muon site, causing a single muon precession frequency observed as spontaneous oscillation of $G_z(t)$ (for reviews of μSR in magnetic materials, see [2]). In cases where the magnetic moments in the material are static (not fluctuating) yet not long-range ordered (as in frozen spin glasses and conductors containing only nuclear moments), the 'Kubo–Toyabe' relaxation functions [3] corresponding to either a Gaussian local field distribution

$$G_z^G(t) = \frac{1}{3} + \frac{2}{3}(1 - \Delta^2 t^2)\exp\left(-\frac{\Delta^2 t^2}{2}\right) \tag{1}$$

(where $\Delta = \gamma_\mu (B_x)_{rms}$, and γ_μ is the muon gyromagnetic ratio) or to a Lorentzian local field distribution

$$G_z^L(t) = \frac{1}{3} + \frac{2}{3}(1 - at)\exp(-at) \tag{2}$$

(where $a = \gamma_\mu (B_x)_{hwhm}$) have been sufficient to fit all data obtained until recently. In both of these functions, polarization drops from the initial value of unity to a single minimum, and

0953-8984/99/061589+12$19.50

then recovers to 1/3 at late times. This 1/3 asymptote is a characteristic feature of muon spin relaxation in static random local fields and zero external field. It is now known, however, that in a small number of materials, including Al–Mn–Si magnetic quasicrystals [4] and $CeNi_{1-x}Cu_xSn$ Kondo-lattice alloys [5], static ZF relaxation of initial polarization can lead to a minimum too shallow to be reproduced by either of the Kubo–Toyabe functions (equation (1) or equation (2)) above. In fact, the extreme case of monotonic decay to the 1/3 asymptote has been observed.

A prior publication [6] showed that the observed relaxation in $CeNi_{1-x}Cu_xSn$ alloys is fitted well by a relaxation function derived from a 'convolution broadening' of a Gaussian distribution. This means that instead of a single-Gaussian random local field distribution with a unique value of $(B_x)_{rms}$, a collection of distributions are used, corresponding to a collection of different muon sites, where the collection of values of $(B_x)_{rms}$ themselves form a Gaussian distribution of width W and most likely value B_0. This 'Gaussian-broadened Gaussian' static ZF Kubo–Toyabe relaxation function has the form

$$G_z^{GBG}(t) = \frac{1}{3} + \frac{2}{3}\left(\frac{1+R^2}{1+R^2+R^2\Delta_{eff}^2t^2}\right)^{3/2}\left(1-\frac{\Delta_{eff}^2t^2}{1+R^2+R^2\Delta_{eff}^2t^2}\right) \times \exp\left(\frac{-\Delta_{eff}^2t^2}{2(1+R^2+R^2\Delta_{eff}^2t^2)}\right) \tag{3}$$

where $\Delta_{eff}^2 = \gamma_\mu^2(B_0^2 + W^2)$ and $R = W/B_0$. Previously, however, no microscopic model of moments in a solid was presented that could produce such a field distribution.

Directly, μSR 'senses' only the magnetic fields at the muon sites, and as such is a local probe that has not been expected to be sensitive to correlation lengths. In cases that require a non-trivial value of R in equation (3), however, that non-trivial value (or, equivalently, the shallowness of the minimum of polarization) is extra information not provided by the standard Gaussian or Lorentzian forms. One publication [4] had speculated that this kind of anomalous relaxation could be produced by random variation of the magnitude of the frozen moments, with a correlation range. The present paper presents the results of Monte Carlo simulations of the ZF muon spin relaxation functions generated by a microscopic model of such 'range-correlated moment magnitude variation' (RCMMV). This involves similar values of the magnitude of nearby magnetic moments that nonetheless have uncorrelated orientations. The results demonstrate that this type of correlation in a magnetically frozen (but disordered) state will generate the kind of shallow static ZF Kubo–Toyabe relaxation function that has been observed for the materials listed above. As the correlation length gets successively larger, the associated relaxation function more closely approaches monotonic relaxation to the 1/3 asymptote, as will be discussed. The extra information represented by the value of R is indeed the range of this correlation. In the model discussed here, this correlation is imposed, not generated by a plausible physical mechanism. The identification of candidate mechanisms is a subject for future research.

Throughout this discussion, it is necessary to understand that while the Lorentzian Kubo–Toyabe relaxation function has a shallower minimum than the Gaussian Kubo–Toyabe function, $G_z^L(t)$ does not fit any data of the type exemplified by the $CeNi_{1-x}Cu_xSn$ data. The Lorentzian case couples that shallower minimum with rapid initial relaxation. If forced to fit the initial relaxation observed in $CeNi_{1-x}Cu_xSn$ [5], the Lorentzian minimum occurs far later than in the data. If forced to fit the observed minimum, the initial decay of $G_z^L(t)$ is much faster than that of the data. The Gaussian-broadened Gaussian function places the minimum at essentially the same time, relative to the initial relaxation, as the standard Gaussian Kubo–Toyabe function, and does fit the data well. Since Gaussian-like behaviour is generally associated with dense-

moment systems [2], a dense array of moments was specifically incorporated into the Monte Carlo model.

2. The microscopic Monte Carlo model

A Monte Carlo simulation of a microscopic model of moments on a lattice has been used before to simulate the field distribution at an interstitial muon site and the corresponding static ZF muon spin relaxation function [7]. For a cluster of a finite number of ions on a lattice, a vector magnetic moment is assigned to each magnetic ion, the assumed coupling of the moments to a muon at a particular site is used to calculate the effective field due to each ion at the muon site, and those individual-ion fields are vector summed to find the net local field at the muon for that particular moment configuration. For any particular initial muon polarization, the precession of the muon spin around the local field is calculated. Of particular interest is the projection of the polarization along its initial direction, as a function of time. This is the longitudinal relaxation function $G_z(t)$. For a single muon, this will oscillate at the Larmor frequency of the local field. If there is any disorder in the system, randomization characteristic of that disorder is included in the calculation, and the calculation is repeated many times. The many net local fields are collected into histograms representative of the local field probability distribution, and the projected polarization of many muons is averaged to generate the simulated static muon spin relaxation function.

One type of disorder that often occurs in samples studied with μSR is polycrystallinity. Most μSR experiments are performed on powders or polycrystalline ingots, where all possible orientations of the principal axes of the crystallites of the material, with respect to the initial muon polarization, occur. This averages over any anisotropy of the relaxation with respect to the crystal axes. All of the equations above assume 'polycrystalline averaging' (or perfect isotropy of the local field distribution). In a Monte Carlo program, this is achieved by randomizing the orientation of the lattice principal axes relative to the initial muon polarization, and this was done in every case in the simulations discussed below.

A previous publication [7] discussed Monte Carlo simulation of the static ZF relaxation functions that should be generated by non-dilute alloys, and that the path to the Lorentzian case in the dilute limit was not simple. That program used fixed-magnitude, random-direction moments in a cluster of lattice positions. Upon discovery of the anomalous, shallow-minima, static ZF relaxation functions, and with the expectation that some new type of disorder would be required in the explanation, a simple modification was made to that program which randomized the moment magnitude in addition to the orientation. The modification produced simulated field distributions and relaxation functions of the same qualitative form as those shown in the earlier paper. They evolved from the Gaussian Kubo–Toyabe function at high moment concentration, through two-minima forms (with two effective sites) at intermediate concentrations, to the Lorentzian limit at low concentrations, without producing anything that fitted the shallow relaxation functions of $CeNi_{1-x}Cu_xSn$ and magnetic Al–Mn–Si quasicrystals. *Completely random moment variation does not explain the anomalous relaxation that has been observed.*

The subject of this paper is a model that more successfully reproduces shallow static ZF relaxation functions. It was constructed to be a specific example of range-correlated moment magnitude variation, alluded to above. Retaining a lattice cluster and completely random moment orientations, moment magnitudes are held fixed in sub-clusters of moments, while they are varied randomly between sub-clusters. Forcing the sub-clusters to have a particular average size creates a correlation range. To obtain good statistical behaviour of the simulations using such sub-clusters, substantially larger overall cluster size is necessary: while the clusters

of the previous Monte Carlo μSR paper [7] were spheres of up to 500 ions on fcc lattice sites, the work reported here used cubes of ions on simple-cubic lattice sites, with up to 126 ions on a side (containing, therefore, up to slightly more than two million ions). The use of cubic clusters, and a simple-cubic lattice, help reduce CPU time, as does the increase in computation speed available since that previous publication. The qualitative conclusions drawn should not depend on the particular lattice used, although fine details may well do so.

Within an overall cluster, the sub-clusters were chosen to be rectangular boxes, with each box's three side lengths chosen randomly between one ion thick and a maximum thickness (the 'cut-off', which controls the correlation range), subject to a simple packing constraint such that, in spite of the randomization, the overall cube is filled by the boxes, with no ions left out. For each box, a single value of the moment magnitude is chosen randomly between zero and unity. This rectangular-box configuration of correlated clusters is not physically likely, but is computationally simple. More realistic methods of generating correlations, usually involving some pairwise nearest-neighbour interaction, would require orders of magnitude more CPU time, which would be prohibitive. Furthermore, no physically reasonable candidate mechanisms for producing such correlations are known at this time. The simulations reported here provide a first glimpse of what RCMMV can do to static ZF relaxation functions.

More challenging, in terms of the microscopic physics, is the assumption of continuous moment variation between zero and a maximum. Ion magnetic moments in solids are usually single valued, and cases of static moment instability are usually discussed in terms of (usually only two) distinct values ('mixed valence'; see, e.g., [8]). A continuous range, or at least a large number of possible values, of moment magnitude seems necessary to generate shallow static ZF relaxation. Use of the models described here with only two possible moment values generates field distributions and relaxation functions clearly representative of two muon sites with two particular rms field values, and does not reproduce the shallow static ZF relaxation observed. The behaviour discussed here might well be generated by the size of the magnetic ion moment taking a distinct and unique value (not just on/off) for each and every different near-neighbour environment that occurs in the material. For a site-substitution alloy like $CeNi_{1-x}Cu_xSn$, this would result in a binomial distribution of moment sizes. Continuous ranges of moment values are a possibility in Kondo screening (see, e.g., [9]), but static spatial inhomogeneity with a continuous range of moment values may not yet have been considered in a Kondo-interaction calculation.

The correlation generated by the modelling should be monitored by a two-point correlation function, which, if it decays exponentially in the distance r between the two points, defines a correlation length. Any moment–moment correlation can only be defined at those discrete values of r that represent the separations of pairs of moments in the lattice cluster. For any such r, there will usually be a number $N(r)$ of pairs of moments, with magnitudes m_i and m_j, for which $r_{ij} = r$. The correlation function chosen was

$$C(r) \equiv \frac{1}{N(r)} \sum_{i,j} (1 - |m_i - m_j|)_{r_{ij}=r}. \tag{4}$$

At a particular r, the sum is over all pairs for which $r_{ij} = r$. In this notation,

$$N(r) \equiv \sum_{i,j} (1)_{r_{ij}=r}.$$

$C(r)$ is unity when all moments are the same size, and 2/3 when the magnitudes are completely random on the unit interval. Figure 1 shows $C(r)$ for a typical simulation run, with an overall cluster thickness of 44 ions and a sub-cluster thickness cut-off of 10 ions. All distances are stated as multiples of the distance between nearest-neighbour moments in the lattice

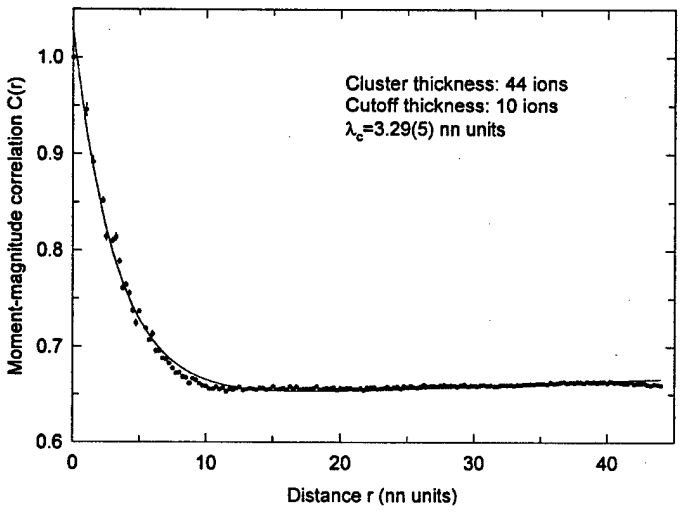

Figure 1. The moment magnitude correlation $C(r)$ (random = 2/3), as a function of distance r between the moments (in units of the distance between nearest-neighbour moments), for a typical Monte Carlo simulation of range-correlated magnetic moment variation (RCMMV, as described in the text), with a cubic cluster thickness of 44 ions, and a rectangular-box sub-cluster cut-off thickness of 10 ions. The solid curve is a fit of exponential decay to the baseline, with a deduced correlation length of 3.29(5).

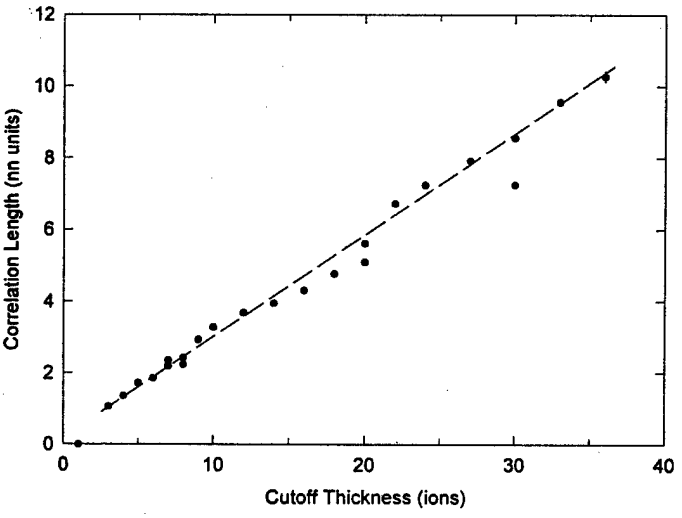

Figure 2. The RCMMV moment magnitude correlation length deduced from fits to $C(r)$ as a function of the sub-cluster cut-off thickness. The straight line (slope 0.29) is a guide for the eye.

(abbreviated as nn). It was found that for runs with cut-off greater than ~1/4 of the overall thickness, the correlation did not settle down near 2/3 for large r, so these were not used. Also shown in figure 1 is the fit of exponential decay to the baseline,

$$C(r) = Ae^{-\lambda_c r} + B \tag{5}$$

(where $A \simeq 1/3$ and $B \simeq 2/3$), with a deduced correlation length $\lambda_c = 3.29 \pm 0.05$ nn. Figure 2 shows the correlation length deduced from such fits as a function of the cut-off

thickness. The correlation length is $\simeq$0.3 times the cut-off thickness. With overall clusters of up to two million ions, correlation lengths only up to about ten times the nn distance can be reasonably modelled.

For each overall cluster, once moment magnitudes were assigned as above, and moment directions randomly, numerous examples of the interstitial muon site (at the crystallographically unique unit-cell centre) were chosen at random from the interior volume at least five nn steps from the outside of the cluster. Modelling of the field distributions and static ZF relaxation functions was then performed as described previously [7]. The local field at each muon site was calculated in dipole coupling to all the moments in the cluster, and then added to the field distribution histograms. The component of muon polarization in its initial direction, as a function of time, was calculated in that local field and added to the relaxation-function histogram. For the larger cluster sizes, typically moments were assigned 600 times and more than 2000 muon sites were evaluated for each of those moment configurations.

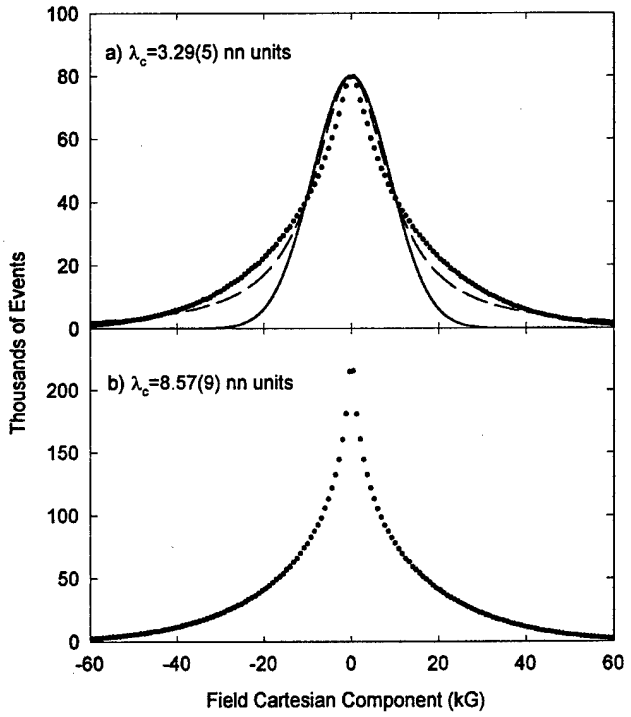

Figure 3. Monte Carlo RCMMV local field Cartesian-component distribution histograms: (a) for an overall thickness of 44 ions and a correlation cut-off thickness of 10 ions; the solid (dashed) curve shows the Gaussian (Lorentzian) distribution with the same maximum and fwhm; (b) for an overall thickness of 126 ions and a correlation cut-off of 30 ions.

3. Results

The Gaussian and Lorentzian Kubo–Toyabe relaxation functions are named after the distributions of one Cartesian component of the magnetic field, $P(B_x)$, that generate them. As previously discussed, however [7], particularly in the case of polycrystalline averaging, the distribution of the magnetic field magnitude $P(|B|)$ is more directly related to the static ZF

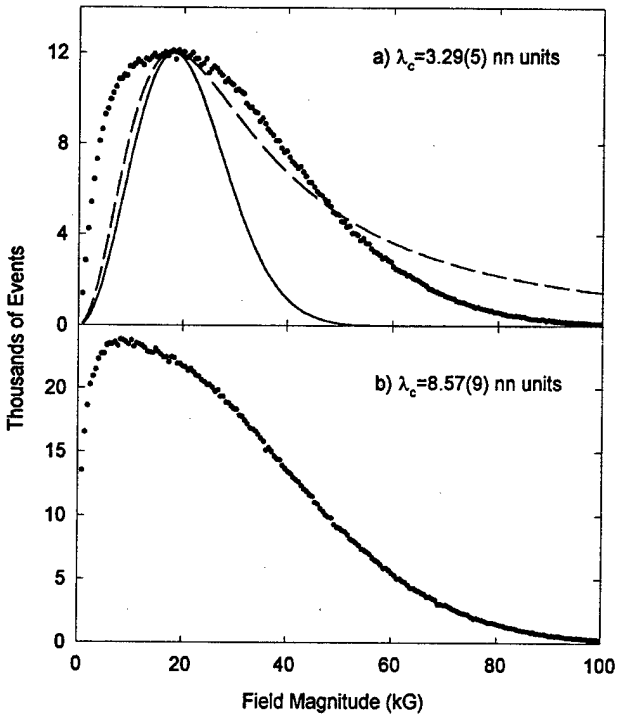

Figure 4. Monte Carlo RCMMV local field magnitude distribution histograms: (a) for an overall thickness of 44 ions and a correlation cut-off thickness of 10 ions; the solid (dashed) curve shows the Maxwellian (Lorentzian [7, 10]) magnitude distribution with same maximum value and position; (b) for an overall thickness of 126 ions and a correlation cut-off of 30 ions.

relaxation function, by

$$G_z(t) = \frac{1}{3} + \frac{2}{3}\int_0^\infty P(|B|)\cos(\gamma_\mu |B| t)\,\mathrm{d}|B|. \tag{6}$$

Therefore both the component and magnitude distributions were monitored by the Monte Carlo program. Examples are shown in figure 3 and figure 4, respectively. For comparison, curves in figure 3 show the Gaussian and Lorentzian distributions with the same fwhm as the simulation: the RCMMV model generates distributions more sharply peaked at low field than either of the standard ones. The curves in figure 4 show Maxwellian and Lorentzian [7, 10] magnitude distributions, and the model clearly generates distributions with more probability of the occurrence of low fields, relative to the most likely field. Figure 5 shows a sequence of simulated static ZF relaxation functions, for the correlation lengths shown. The simulation shown for no correlation (every moment magnitude and direction random) is almost indistinguishable from the standard Gaussian Kubo–Toyabe function. The model, as described, naturally keeps the average moment (magnitude) per unit volume constant, independently of the correlation length, and this results in a constant rms local field Cartesian component $(B_x)_{rms}$. For moments in the interval (0, 1 μ_B) at 1 Å spacing, as shown for figures 3 and 4, $(B_x)_{rms} = 19.8 \pm 0.2$ kG. As a further result, it can be seen in figure 5 that the initial drop of polarization from 1.0 to ~0.6 is also essentially independent of the correlation, and that the time at which minimum polarization occurs is not strongly dependent on the correlation, but that the value of minimum polarization achieved increases with λ_c. Figure 6 shows the minimum polarization of the Monte Carlo relaxation functions, plotted as a function of $1/\lambda_c$.

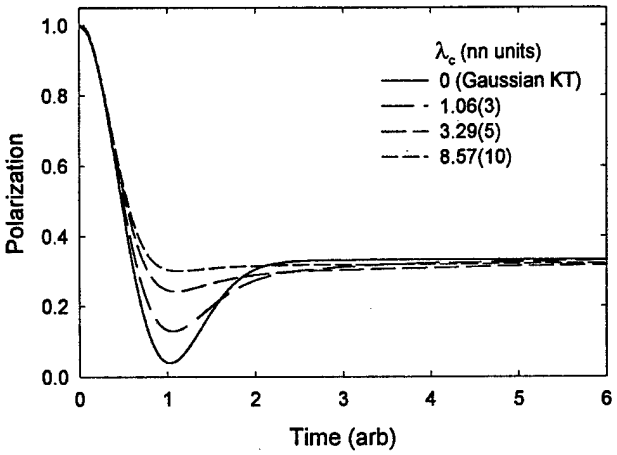

Figure 5. Monte Carlo RCMMV static ZF muon spin relaxation functions for the moment magnitude correlation lengths indicated.

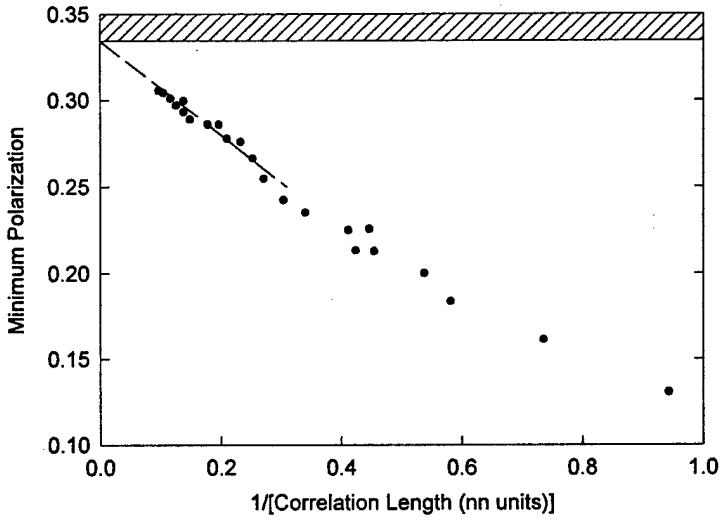

Figure 6. The minimum polarization achieved by the Monte Carlo RCMMV static ZF muon spin relaxation functions, as a function of the reciprocal of the moment magnitude correlation length λ_c. The horizontal line represents the 1/3 asymptote, above which the minimum polarization cannot rise. The dashed line is a guide for the eye.

Comparison of the simulated relaxation with the Gaussian-broadened Gaussian analytic form (equation (3)) can be made by treating each Monte Carlo spectrum as data and fitting $G_z^{GBG}(t)$ to it, as shown in figure 7. The fits are reasonable, but not perfect. Figure 8 shows that the deduced GBG ratio parameter R appears to have a simple straight-line relationship with the reciprocal of the correlation length, $1/\lambda_c$.

The RCMMV simulated relaxation cannot be properly least-squares fitted to experimental data, because only discrete values of the cut-off (and hence, the correlation length) are available. Figure 9 shows a comparison of simulated RCMMV for $\lambda_c = 2.94$ nn and low-temperature ZF μSR in $CeCu_{0.2}Ni_{0.8}Sn$ [5, 6]. The agreement between the two is fairly good.

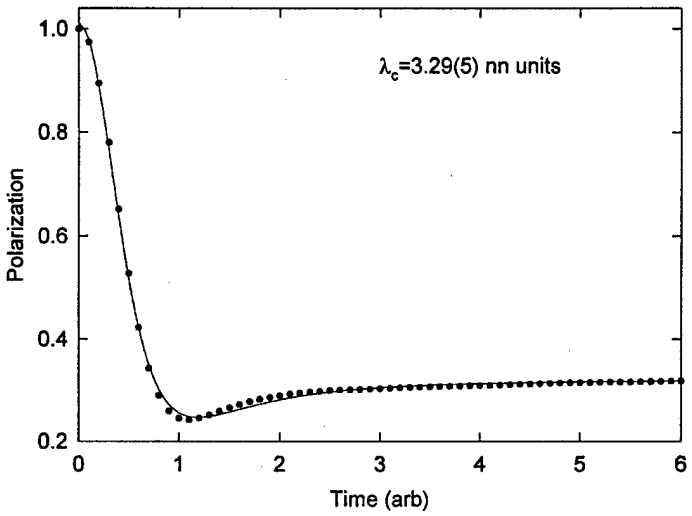

Figure 7. The Monte Carlo RCMMV static ZF muon spin relaxation function for a cluster overall thickness of 44 ions and a correlation cut-off thickness of 10 ions (circles), with a fit of a Gaussian-broadened Gaussian relaxation function (curve). The deduced GBG ratio parameter is $R = 0.543(6)$.

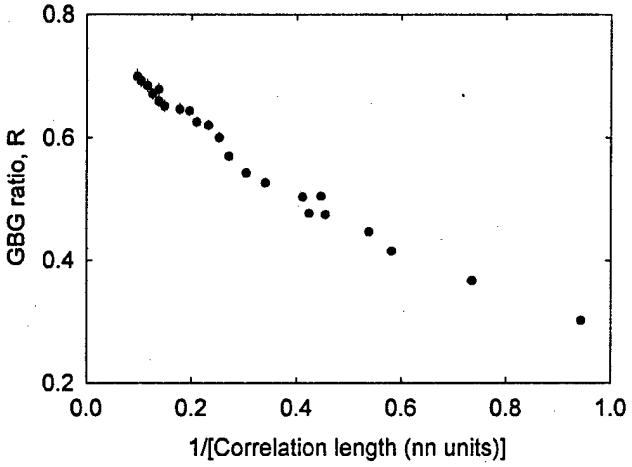

Figure 8. The GBG ratio parameter R, deduced from fits to Monte Carlo RCMMV static ZF μSR spectra, as a function of $1/\lambda_c$.

4. Discussion

The Monte Carlo model is crude in several respects, one of which is the forced total lack of correlation beyond the sub-cluster thickness cut-off parameter value. Thus (figure 1) it can only approximate the exponential decay of correlation with distance to be expected in a real situation. Nonetheless it shows that RCMMV can generate arbitrarily shallow static ZF relaxation functions. There is at this time no other microscopic model known to do so.

The field distributions generated by the RCMMV Monte Carlo model have dramatically enhanced probabilities of low fields relative to those of the average (or rms) fields of the

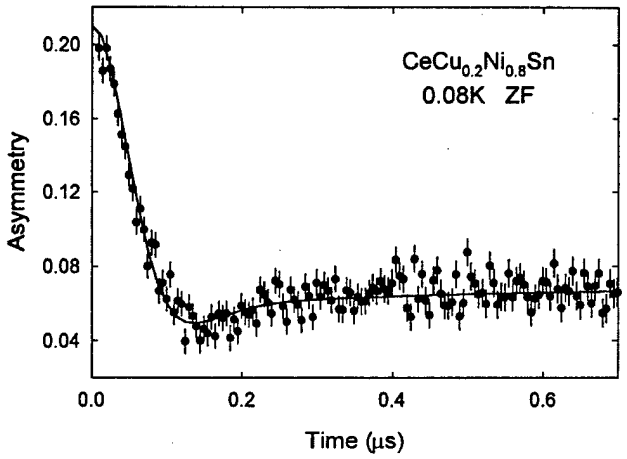

Figure 9. Comparison of the Monte Carlo RCMMV relaxation function having correlation length $\lambda_c = 2.94$ nn to the low-temperature ZF μSR observed in $CeCu_{0.2}Ni_{0.8}Sn$.

standard field distributions. As illustrated in figure 3, $P(B_x)$ becomes progressively more sharply peaked around $B_x = 0$ as the correlation length increases. In figure 4, meanwhile, the most likely field magnitude shifts to progressively lower values relative to the high-field tail of $P(|B|)$. A strictly phenomenological form which roughly fits the magnitude distributions is

$$P_z^{phen}(B) = \frac{N}{\mathcal{W}}\left(\frac{B}{\mathcal{W}}\right)^p \exp\left(\frac{-B^2}{2\mathcal{W}^2}\right) \tag{7}$$

where $\mathcal{W}$ is a width parameter. The power p is close to 2 for $\lambda_c = 0$ (where the simulation magnitude distribution is almost indistinguishable for the Maxwellian case, and $\mathcal{W} = (B_x)_{rms}$), but decreases as λ_c increases. A graph of p as a function of $1/\lambda_c$ suggests that in the limit of long correlation length, $p \to 0$; that is, the magnitude distribution would be approximately Gaussian (with $\mathcal{W} = |B|_{rms}$). No such closed-form approximation has yet been found for $P(B_x)$.

Note that the relaxation function $G_z(t)$, as determined from equation (3), is (a constant plus) the cosine Fourier transform of $P(|B|)$. From this, the (extrapolated) change of the magnitude distribution from possessing a peak at non-zero field to possessing a peak only at $|B| = 0$, as $\lambda_c \to \infty$, implies a change in G_z from underdamped (possessing a local minimum) to overdamped (showing monotonic relaxation to the asymptote) in that limit. Similarly, the extrapolation of the minimum polarization on figure 6 suggests that the local minimum disappears into the 1/3 asymptote for infinite λ_c. It thus appears that the complete range of shallow minima, down to vanishingly small, is spanned by this model.

The extrapolation of the Gaussian-broadened Gaussian ratio R, in figure 8, however, suggests a limit value for R of slightly less than 0.8, which still implies a small local minimum of polarization. The fits of G_z^{GBG} to the Monte Carlo relaxation functions are not perfect, and, to fit the Monte Carlo initial relaxation better, overestimate the depth of the minimum for the larger-λ_c cases. This discrepancy may be due to the crudeness of the Monte Carlo model (but that idea can only be tested by developing models that are more realistic). It would be nice to be able to use figure 8 as a calibration curve for conversion of measured GBG ratio values to underlying correlation lengths, but the imperfect match of $G_z^{GBG}(t)$ to the RCMMV Monte Carlo relaxation functions limits confidence in this. Direct comparison of individual simulations to observed data is useful, but is not as impartial as least-squares fitting is: there

is a risk of systematic personal bias in the deduced parameter values. For the data of figure 9, since the simulation for $\lambda_c = 3.29$ nn looks almost as good as the 2.94 nn case shown, it is reasonable to conclude that $\lambda_c = 3.1 \pm 0.3$ nn.

Care must be exercised in thinking about the statistics of the model in the large-correlation-length limit, '$\lambda_c \rightarrow \infty$'. In this limit, $C(r)$ becomes unity, and it would seem that all moments are the same size, which is a case well known to generate a relaxation function well approximated by the Gaussian Kubo–Toyabe function, not the monotonic relaxation to 1/3 asserted above. The difference is that for any finite r, no matter how large, as many muons will find sites surrounded by very small moments as will land at sites with moments near the maximum value. For all finite r, the moments are uniformly spread over the unit interval. This is only a formal problem. Physically, a correlation length $\lambda_c \sim 30$ nn units (typically less than 200 Å in real materials) would generate a static relaxation function with a minimum so shallow that it would be well approximated by monotonic relaxation, within the statistical accuracy of a normal μSR spectrum, and thus would appear to be at the limit, yet with sample dimensions of at least tenths of millimetres, there will still be room for millions of such correlated regions with vastly different moment magnitudes.

5. Conclusions

The observed anomalous form (with the characteristic shallow minimum) of static ZF muon spin relaxation in disordered magnetic materials such as $CeNi_{1-x}Cu_xSn$, which was previously found to conform to the phenomenological 'Gaussian-broadened Gaussian' relaxation function, has been shown here, by Monte Carlo simulation, to be associated with a subtle short-range partial-ordering effect: range-correlated moment magnitude variation (RCMMV). The shallowness of the ZF relaxation, relative to standard Gaussian Kubo–Toyabe relaxation, is in a one-to-one relationship with the moment magnitude correlation length, and so μSR, as a local probe, in these circumstances provides a measure of a correlation length. It is a strange and heretofore unexpected correlation, however, of static spatial inhomogeneity of the moment magnitudes: the moments not just 'on' or 'off', but ranging over enough distinct values to be approximated by a continuous range from zero to a maximum.

Acknowledgments

Thanks to G M Kalvius and C E Stronach for their suggestions and encouragement. This work was supported by US Air Force Office of Scientific Research grant F49620-97-1-0297 and Ballistic Missile Defence Organization grant F49620-97-1-0532.

References

[1] Schatz G and Weidinger A 1992 *Nukleare Festkörperphysik* 2nd edn (Stuttgart: Teubner) (Engl. Transl. 1996 *Nuclear Condensed Matter Physics* (Chichester: Wiley))
Karlsson E B 1995 *Solid State Phenomena as Seen by Muons, Protons, and Excited Nuclei* (Oxford: Oxford University Press)
[2] Schenck A and Gygax F N 1995 *Handbook on Magnetic Materials* vol 6, ed K H J Buschow (Amsterdam: Elsevier) p 57
Dalmas de Réotier P and Yaouanc A 1997 *J. Phys.: Condens. Matter* **9** 9113
[3] Kubo R and Toyabe T 1967 *Magnetic Resonance and Relaxation* ed R Blinc (Amsterdam: North-Holland) p 810
[4] Noakes D R, Ismail A, Ansaldo E J, Brewer J H, Luke G M, Mendels P and Poon S J 1995 *Phys. Lett.* A **199** 107

[5] Kalvius G M, Flaschin S J, Takabatake T, Kratzer A, Wäppling R, Noakes D R, Burghart F J, Brückl A, Neumaier K, Andres K, Kadono R, Watanabe I, Kobayashi K, Nakamoto G and Fujii H 1997 *Physica* B **230–232** 655
[6] Noakes D R and Kalvius G M 1997 *Phys. Rev.* B **56** 2352
[7] Noakes D R 1991 *Phys. Rev.* B **44** 5064
[8] Müller-Hartmann E, Roden B and Wolleben D (ed) 1984 *Proc. 4th Int. Conf. on Valence Fluctuations* (Amsterdam: North-Holland)
[9] Hewson A C 1993 *The Kondo Problem to Heavy Fermions* (Cambridge: Cambridge University Press)
[10] Kubo R 1981 *Hyperfine Interact.* **8** 731

2 February 1998

PHYSICS LETTERS A

ELSEVIER

Physics Letters A 238 (1998) 197–202

Spin dynamics and freezing in magnetic rare-earth quasicrystals

D.R. Noakes [a,1], G.M. Kalvius [b], R. Wäppling [c], C.E. Stronach [a], M.F. White Jr. [a], H. Saito [d], K. Fukamichi [d]

[a] *Physics Department, Virginia State University, Petersburg, VA 23806, USA*
[b] *Physik Department-E15, Technische Universität München, D-85747 Garching, Germany*
[c] *Physics Department, Uppsala University, Box 530, S-751 21 Uppsala, Sweden*
[d] *Department of Materials Science, Faculty of Engineering, Tohoku University, Sendai 980-77, Japan*

Received 11 November 1997; accepted for publication 14 November 1997
Communicated by L.J. Sham

Abstract

Muon spin relaxation measurements of $RE_8Mg_{42}Zn_{50}$ (RE = Gd, Tb) quasicrystals have revealed slower spin dynamics and more prompt spin freezing for Tb than Gd, due to "crystalline electric field" splitting in low rare-earth site symmetry. Inhomogeneous spin freezing leads to a low-temperature state with local field distribution characteristic of a concentrated disordered magnet. © 1998 Elsevier Science B.V.

PACS: 75.50.Kj; 76.75.+i
Keywords: 4*f* magnetism; Spin-glass freezing; Icosahedral

Among all of the quasicrystalline materials [1], magnetism has been fairly rare. Recently, the icosahedral (*i*-) RE-Mg-Zn (RE = rare earth) series was discovered [2,3], offering the chance to study the behavior of rare-earth magnetic ions in a quasicrystalline environment, and to compare rare-earth quasicrystals with those containing 3d magnetic ions (e.g., *i*-Al-Mn-Si). Of particular interest are the thermodynamically stable *i*-$RE_8Mg_{42}Zn_{50}$ phases, which have spin-glass-like freezing temperatures (T_g) below 10 K. Recently, neutron scattering studies have shown evidence of magnetic quasilattice ordering in several of these near 20 K [4], where there is, strangely, no indication of a transition from any other probe.

Muon spin relaxation (μSR) (see introductory reviews [5]) has been applied successfully to the study of spin dynamics in spin glasses and other disordered magnetic structures (see, e.g., Refs. [8,9]). The relaxation function in zero applied field (ZF) for an isotropic random spin arrangement is known as the Kubo–Toyabe function [10]. Usually, for a *static* spin system, the muon spin polarization decays from its initial value (A_0) at early times, but at later times returns to an $A_0/3$ asymptote. The shape of early depolarization reflects the nature of the distribution of local fields at the μ^+ site, and its rate is proportional to the half-width of that distribution. For a dilute spin glass, the field distribution is Lorentzian; for a dense array of random moments it is Gaussian. In the Gaussian case, slow spin dynamics cause decay of the $A_0/3$ asymptote and increasingly faster fluctuations eventually lead to monotonic exponential relaxation with decreasing relaxation rate (motional "narrowing" is decoupling

[1] E-mail: DNoakes@VSU.edu.

PII S0375-9601(97)00888-8

here). For a Lorentzian field distribution, if dynamics allowed each muon to sample the entire distribution, there would only be decay of the $A_0/3$ asymptote and no change in overall depolarization rate. This, however, is not true for dilute spin glasses: as shown by Uemura et al. [8], a single muon can only see a limited portion of the complete Lorentzian distribution, with the result that in the fast fluctuation limit there is decoupling, with "root-exponential" ($\exp(-\sqrt{\lambda t})$) line shape. Careful study of the μSR response can provide detailed information on the microscopic properties of magnetically disordered materials.

Previous μSR studies of the spin-glass behavior of *i*-Al-Mn-Si [6] found that inhomogeneous freezing persists at all temperatures below T_g, together with an anomalously-broad local field distribution in the frozen regions [7]. In the present μSR studies poly-quasicrystalline ingots of *i*-$Gd_8Mg_{42}Zn_{50}$ and *i*-$Tb_8Mg_{42}Zn_{50}$, with reported T_g's near 6 K and 8 K, respectively [2,3], were used. The measurements were performed with "surface" muons at TRIUMF in two sets, the first covering $3\text{ K} \leqslant T \leqslant 200$ K, the second in a dilution refrigerator for temperatures down to ~100 mK in connection with up to 2.5 T longitudinal field (LF, i.e. applied parallel to the initial muon polarization). We will discuss the two sets separately.

Both rare-earth quasicrystal samples showed two distinctly different signals at all temperatures. One involved *temperature-dependent* muon spin relaxation, as expected for a material with paramagnetic ions that freeze. The other was very weakly relaxing (near the limit of detection) and *temperature independent*. Its amplitude was too large to be only from muons stopped outside the sample (in the sample holder, cold finger, etc.) although such a background signal is certainly contained within it. This non-relaxing signal is difficult to interpret when X-ray diffraction indicates the samples are single-phase. Such weak muon spin relaxation can be seen in a paramagnet if either there is an extremely small r.m.s. local field at the muon site (in this case, that would be in a region of unexpectedly low rare-earth ion concentration), or if the local field fluctuates so rapidly it causes almost complete motional decoupling (which is very unlikely at temperatures below T_g, where this signal is still seen). We have at this stage no definitive explanation. Interestingly, a similar weakly-relaxing temperature-independent fraction was also seen in μSR of the manganese-containing magnetic quasicrystal *i*-Al-Mn-Si [6]. Since the non-relaxing signal is independent of temperature and applied field, it does not interfere with the analysis of the fast-relaxing signal, which reflects the magnetic properties of the samples.

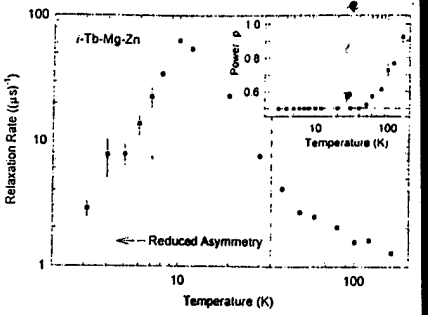

Fig. 1. Temperature dependence of the near-ZF muon spin relaxation rate, r, in *i*-$Tb_8Mg_{42}Zn_{50}$, on double logarithmic scales. The vertical dashed line indicates the onset of loss of asymmetry at low temperatures. The inset shows the temperature dependence of the power, p, on semi-logarithmic scales. T_g is near 8 K.

In ZF, the fast-relaxing μSR signal in $Tb_8Mg_{42}Zn_{50}$ could be fit in the paramagnetic regime ($T > T_g$) as "power-exponential" relaxation,

$$A(t) = A_0 \exp[-(rt)^p]. \quad (1)$$

Such a power-exponential μSR signal has been observed in a number of disordered magnetic materials [11]. Fig. 1 shows the temperature dependence of the relaxation rate, r, and the power, p. The latter drops (while r increases) from $p \approx 1$ (simple exponential) at 180 K to $p = 0.5$ (root-exponential) at ~ 40 K. Below 30 K, A_0 begins to decrease because the initial relaxation has become so fast that the early part of the signal is lost in the initial dead time (~ 8 ns) of the μSR spectrometer. Under these circumstances, the least-squares fit can no longer reliably determine the value of p, so we have fixed it at $p = 0.5$. Below 10 K, with detected signal amplitude reduced to about 1/3 of its high-temperature value, the relaxation rate began to decrease as temperature decreased, which we interpret below as due to slow fluctuations in the spin-frozen state. Qualitatively similar behavior was observed, e.g., in amorphous DyAg [12].

Corresponding μSR spectra from the paramagnetic state of *i*-$Gd_8Mg_{42}Zn_{50}$ showed, contrastingly, a sim-

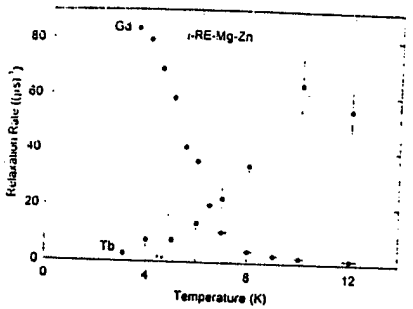

Fig. 2. Temperature dependence of the near-ZF muon spin relaxation rate in i-$Gd_8Mg_{42}Zn_{50}$ (circles), on linear scales. Nominal T_g is near 6 K. For ease of comparison, the corresponding points for the Tb quasicrystal are also shown (triangles). Full asymmetry was resolved for the Gd data shown, while Tb asymmetry was severely reduced in this temperature range.

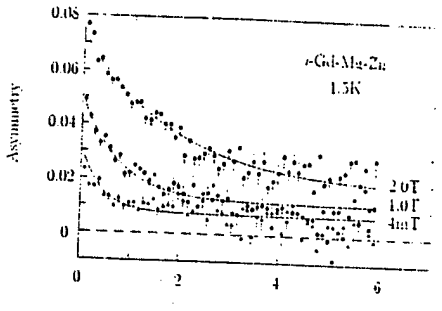

Fig. 3. μSR asymmetry spectra of i-$Gd_8Mg_{42}Zn_{50}$ at 1.5 K, in the applied longitudinal fields shown. The solid lines are a least-squares fit of a spin-freezing model described in the text. The asymmetry scale ignores the non-relaxing signal.

ple exponential fast-relaxing signal at much lower rates than in the Tb sample, rising from $0.56(\mu s)^{-1}$ at 195 K to $1.4(\mu s)^{-1}$ at 12 K (see Fig. 2). Changes in shape below 12 K are associated with inhomogeneities in the spin-freezing process, as will be discussed below. Full instrumental asymmetry was resolved down to 4.5 K, but then some of the extremely fast relaxation was lost in the initial dead time for this sample, as well. The temperature dependence of the Gd-quasicrystal relaxation in Fig. 3 suggests T_g perhaps as high as 7 K. In neither sample, however, is there any indication of a transition at $\sim$ 20 K as reported by neutron scattering [4], nor was any spontaneous spin precession (the classic μSR indicator of long-range magnetic order) observed.

The striking differences in the μSR observed in these two samples are: (i) the substantially larger relaxation rate in the Tb quasicrystal than in the Gd one, and (ii) the power-exponential shape of the relaxation function of the Tb quasicrystal, compared to simple exponential ($p = 1$) for the Gd quasicrystal down to near T_g. The rapidly-fluctuating fields in an unfrozen paramagnet generate relaxation rate $r = \gamma_\mu^2 \langle B_\mu^2 \rangle \tau$ in Eq. (1), where γ_μ is the muon gyromagnetic ratio ($\gamma_\mu/2\pi = 135.5$ MHz/T), $\langle B_\mu^2 \rangle$ the second moment of the field distribution at the muon site (the mean field being zero in ZF) and $1/\tau$ is the field fluctuation rate. For a particular μ^+ site, $\langle B_\mu^2 \rangle$ is determined by the magnitude of the surrounding moments. For Tb^{3+} and Gd^{3+}, the free-ion moments are comparable, so the large difference in relaxation rates implies a lower Tb fluctuation rate. This, we believe, arises from the Tb single-ion anisotropy and level splitting caused by crystalline electric fields (CEF), relative to gadolinium's S-state (unaffected by CEF multipoles) isotropy and degeneracy of J_z sub-states. For low magnetic freezing temperatures, paramagnetic moment fluctuation rates can be strongly suppressed when temperatures fall below the highest energy CEF-split levels of a non-S ion such as Tb in a low-symmetry site (see Ref. [13]). Very similar high muon relaxation rates for (non-S) Ho, compared to the much lower rates for Gd, were observed in the paramagnetic states of $RERh_4B_4$ materials [14], where the Ho CEF splittings are known to be much larger than the magnetic ordering temperature [15]. Heat capacity measurements [3] have indicated that the Tb magnetic sublevels are substantially split, and that the ground state is a doublet or triplet. Charrier et al. [4], on the contrary, argue that the icosahedral symmetry is nearly spherical and CEF effects are expected to be small. Our results quite definitely show the rare-earth site symmetry to be low, and that CEF effects are important.

Next, we consider the difference in shape of the relaxation in the two samples. Campbell et al. [11] argue that power-exponential μSR, as seen in our Tb quasicrystal, is related to "stretched exponential" relaxation of bulk response in some spin glasses [16], but did not establish a detailed connection. We note

that in all cases of power-exponential μSR, $p = 1$ is approached as the temperature (and with it the fluctuation rate) is increased far enough above T_g. The fact that $p = 1$ is seen in i-Gd-Mg-Zn down to temperatures close to T_g seems likely to be related to its higher fluctuation rate (and thus again to the absence of local anisotropy). In many rare-earth intermetallics it is observed that paramagnetic fluctuations remain fast until close to the transition temperature for the Gd member, while for rare-earth ions with high anisotropy, spin dynamics slow down at much higher temperatures (typical examples are $REGa_6$ [17] and $RENi_5$ [18]).

Our assertion that the difference in μSR between the Tb and Gd quasicrystals is due primarily to greatly different moment fluctuation rates is supported by measurements at dilution-refrigerator temperatures. Below 3 K, the ZF resolved amplitude in $Gd_8Mg_{42}Zn_{50}$ drops (as it does in the Tb sample at higher temperatures), as the fast-relaxing signal becomes lost in the initial dead time, and what little is resolved relaxes more slowly as temperature decreases. Thus, far enough below T_g, where the Gd moments approach a static configuration, the μSR spectra begin to look like those of the Tb quasicrystal. Such small-amplitude, slowly relaxing signals from near-ZF μSR by themselves, however, do not provide much information on the frozen magnetic state.

To gain more information, we applied large longitudinal fields. Fig. 3 shows LF-μSR spectra from $Gd_8Mg_{42}Zn_{50}$ at 1.5 K: the overall relaxation rate is lowered, and asymmetry that had been lost in the dead time at low fields is recovered. To our knowledge, this is the first successful application of LF to recover signal loss in the μSR initial dead time. The LF spectra were fit with an inhomogeneous-freezing model. Part of the volume of the sample possesses a rapidly fluctuating, "unfrozen" spin system which shows exponential relaxation unaffected by the applied field (this puts fluctuation rates at least in the GHz regime). The other part of the volume is mildly inhomogeneous in its freezing, meaning that its muon spin relaxation signal is described by the Gaussian Kubo–Toyabe relaxation, part of which is completely static, part of which has a local-field fluctuation rate of less than $5(\mu s)^{-1}$ (which is really very slow). The static and slow-fluctuating parts decouple in LF as shown by the solid lines in Fig. 3 (and in Fig. 4 described below). At 5 K, almost all the moments are still rapidly fluctuating, and even 2 T LF has little effect. Between 5 K and 1.5 K, inhomogeneous freezing occurs, and finally the "unfrozen" signal is no longer present at 1.5 K.

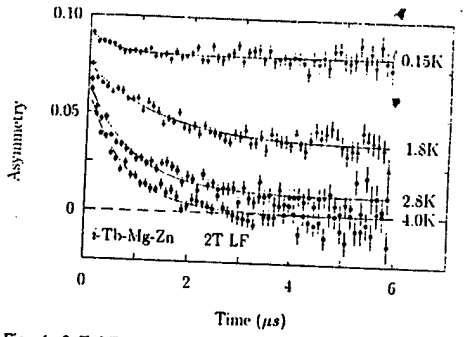

Fig. 4. 2 T LF-μSR asymmetry spectra of i-$Tb_8Mg_{42}Zn_{50}$ at the temperatures shown. The solid lines are a least-squares fit of the same model as Fig. 3. The asymmetry scale ignores the non-relaxing signal.

In $Tb_8Mg_{42}Zn_{50}$, 1 T and 2 T LF at 4 K do cause partial decoupling in a manner similar to that shown in Fig. 3 for Gd at 1.5 K. Therefore, if there is any temperature range of inhomogeneous freezing in this sample, it lies above 4 K. Fig. 4 shows the evolution of 2 T LF-μSR in the Tb quasicrystal: as temperature decreases the volume of utterly static moments increases, and the (slow) fluctuation rate, where there are such fluctuations, also decreases. A qualitatively similar behavior is observed for the frozen-region signal in $Gd_8Mg_{42}Zn_{50}$. Fits to all the low temperature LF-μSR data are consistent with a Gaussian-like distribution of the local field in the frozen state, with $B_{rms} \sim 1$ T, a reasonable size for dipole coupling to the density of rare-earth moments in these samples. This corresponds to $\Delta = \gamma_\mu B_{rms} \sim 700(\mu s)^{-1}$, which explains why the early ZF relaxation is completely lost in the instrumental dead time. The precise form of the local field distribution, however, is not completely determined by the data.

The earlier μSR measurements of i-Al-Mn-Si [6] showed that, despite Mn ion concentrations of order 20 per hundred, and a free-ion Mn moment of order half that of the rare earths studied here, the static low-temperature frozen-state ZF signal decouples in longitudinal fields an order of magnitude smaller than necessary for these rare-earth quasicrystals, implying

a correspondingly smaller B_{rms} at the muon site. The fact that the Mn ion moments are fluctuating so fast that they are completely decoupled from the muon above $\sim 2T_g$ is similar to μSR in classic dilute spin glasses such as 1%Mn in copper [8], but the frozen-state field distribution in *i*-Al-Mn-Si does not go to the Lorentzian dilute limit, displaying instead an anomalous form [7]. The μSR of the rare-earth quasicrystals, with "only" 8 magnetic ions per hundred, is more analogous in this respect to more concentrated disordered magnetic systems. Coupling to the muon extends to temperatures far above $2T_g$ (see Ref. [19]), and power-exponential muon relaxation occurs.

In conclusion, we have determined the spin dynamics in the quasicrystals $Gd_8Mg_{42}Zn_{50}$ and $Tb_8Mg_{42}Zn_{50}$. The substantially larger muon relaxation rate in the paramagnetic state of the Tb sample is attributed to a much slower Tb moment-fluctuation rate, due to crystalline electric field splittings originating from the low rare-earth site symmetry. This in turn leads to differences in paramagnetic relaxation shape: power-exponential for Tb, simple exponential for Gd. There is no indication of any transition near 20 K for either sample, in contrast to neutron scattering results [4] which claim the onset of quasilattice magnetic order. Below T_g, a temperature range of inhomogeneous freezing is observed in the Gd quasicrystal. Below roughly 2 K, the magnetic spins are completely frozen, with some very slow fluctuations persisting in a "mildly" inhomogeneous way. The Tb quasicrystal exhibits complete magnetic freezing at 4 K (again with mild inhomogeneity). The local field distribution is at least roughly Gaussian in shape for both samples, with *rms* field of order 1 T. The μSR response in these rare-earth quasicrystals is for the most part consistent with "concentrated" disordered magnetism, whereas previously measured μSR in *i*-Al-Mn-Si is at best only somewhat consistent with dilute spin-glass behavior, with unexplained Mn moments, and an anomalous frozen-state field distribution.

We wish to thank E.J. Ansaldo, C.U. Jackson, B. Hitti, S.R. Kreitzman and M. Good for their assistance in these measurements. X-ray diffraction checks of phase purity were carried out by Yvonne Andersson. This work was supported in part by US DOE grant DE-FG05-88ER45353, US AFOSR grant F49620-97-1-0297, BMBF (Germany) Contract 03-KA-TU-19, the NRF of Sweden, and the NRC of Canada through its support of TRIUMF.

References

[1] C. Janot, Quasicrystals, a primer (Oxford Univ. Press, Oxford, 1992);
A.I. Goldman, R.F. Kelton, Rev. Mod. Phys. 65 (1993) 213.
[2] A. Niikura, A.P. Tsai, A. Inoue, T. Matsumoto, Phil. Mag. Lett. 69 (1994) 351;
Y. Hattori, A. Niikura, A.P. Tsai, A. Inoue, T. Matsumoto, K. Fukamichi, H. Aruga-Katori, T. Goto, J. Phys. Cond. Matter 7 (1995) 2313.
[3] Y. Hattori, K. Fukamichi, K. Suzuki, A. Niikura, A.P. Tsai, A. Inoue, T. Matsumoto, J. Phys. Cond. Matter 7 (1995) 4183.
[4] B. Charrier, D. Schmitt, J. Magn. Magn. Mater. 171 (1997) 106;
B. Charrier, B. Ouladdiaf, D. Schmitt, Phys. Rev. Lett. 78 (1997) 4637.
[5] G. Schatz, A. Weidinger, Nukleare Festkörperphysik, 2nd ed. (B.G. Teubner, Stuttgart, 1992), English translation: Nuclear Condensed Matter Physics (Wiley, Chichester, 1996);
E.B. Karlsson, Solid State Phenomena as Seen by Muons, Protons, and Excited Nuclei (Oxford Univ. Press, Oxford, 1995).
[6] D.R. Noakes, P. Mendels, Hyperfine Int. 85 (1994) 299;
D.R. Noakes, A. Ismail, E.J. Ansaldo, J.H. Brewer, G.M. Luke, P. Mendels, S.J. Poon, Phys. Lett. A 199 (1995) 107.
[7] D.R. Noakes, G.M. Kalvius, Phys. Rev. B 56 (1997) 2352.
[8] Y.J. Uemura, T. Yamazaki, D.R. Harshman, M. Senba, E.J. Ansaldo, Phys. Rev. B 31 (1985) 546;
H. Pinkvos, A. Kalk, C. Schwink, Phys. Rev. B 41 (1990) 590.
[9] G.M. Kalvius, A. Kratzer, D.R. Noakes, K.H. Münch, R. Wäppling, H. Tanaka, T. Takabatake, R.F. Kiefl, Europhys. Lett. 29 (1995) 501.
[10] R. Kubo, T. Toyabe, in: Magnetic Resonance and Relaxation, ed. R. Blinc (North-Holland, Amsterdam, 1967) p. 810.
[11] I.A. Campbell, A. Amato, F.N. Gygax, D. Herlach, A. Schenck, R. Cywinski, S.H. Kilcoyne, Phys. Rev. Lett. 72 (1994) 1291;
A. Keren, P. Mendels, I.A. Campbell, J. Lord, Phys. Rev. Lett. 77 (1996) 1386.
[12] G.M. Kalvius, L. Asch, D.R. Noakes, R. Keitel, J.H. Brewer, E.J. Ansaldo, F.J. Litterst, B. Boucher, J. Chappert, A. Yaouanc, T. Yamazaki, K. Nagamine, K. Nishiyama, O. Hartmann, R. Wäppling, Hyperfine Int. 31 (1986) 303.
[13] D.R. Noakes, J.H. Brewer, D.R. Harshman, E.J. Ansaldo, C.Y. Huang, Phys. Rev. B 35 (1987) 6597.
[14] D.E. MacLaughlin, S.A. Dodds, C. Boekema, R.H. Heffner, R.L. Hutson, M. Leon, M.E. Schillaci, J.L. Smith, J. Magn. Magn. Mater. 31–34 (1983) 497.
[15] B.D. Dunlap, L.N. Hall, F. Behroozi, G.W. Crabtree, D. Niarchos, Phys. Rev. B 29 (1984) 6244.

[16] R.G. Palmer, D.L. Stein, E. Abrahams, P.W. Anderson, Phys. Rev. Lett. 53 (1984) 958;
A.T. Ogielski, Phys. Rev. B 32 (1985) 7384;
J. Souletie, J. Appl. Phys. 75 (1994) 5512.
[17] E. Lidström, R. Wäppling, O. Hartmann, M. Ekström, G.M. Kalvius, J. Phys. Cond. Matter 8 (1996) 6281.
[18] P. Dalmas de Réotier, J.P. Sanders, A. Yaouanc, S.W. Harr
O. Hartmann, E. Karlsson, R. Wäppling, D. Gignoux,
Georges, D. Schmitt, P. L'Héritier, A. Weidinger, P.C.M
Gubbens, Hyperfine Int. 64 (1990) 389.
[19] E.J. Ansaldo, D.R. Noakes, J.H. Brewer, S.R. Kreitzma
J.K. Furdyna, Phys. Rev. B 38 (1988) 1183.

Handbook on the Physics and Chemistry of Rare Earths
Vol. 32
edited by K.A. Gschneidner, Jr., L. Eyring and G.H. Lander

Chapter 206

μSR STUDIES OF RARE-EARTH AND ACTINIDE MAGNETIC MATERIALS*

G.M. KALVIUS
Physics Department, Technical University Munich, 85747 Garching, Germany

D.R. NOAKES
Department of Physics, Virginia State University, Petersburg, VA 23806, USA

O. HARTMANN
Department of Physics, University of Uppsala, 75121 Uppsala, Sweden

Contents

List of symbols 58
List of acronyms 59
1. Introduction 60
2. The μSR technique 62
2.1. General aspects 62
2.2. Properties of the muon 66
2.3. Muon generation and decay 67
2.4. Muon implantation 69
2.5. Muon beam characteristics 71
2.6. The recording of μSR spectra 76
2.7. Special applications 81
2.7.1. Extreme temperatures 81
2.7.2. High magnetic fields 82
2.7.3. High pressure 83
2.7.4. Small samples 85
2.7.5. Low-energy muons 86
3. μSR magnetic response 88
3.1. The local field at the muon site 88
3.2. μSR spectroscopy of dia- and paramagnets 92
3.2.1. Transverse field measurements (Knight shift) 93
3.2.2. Zero field measurements 97
3.2.3. Longitudinal field measurements 102
3.3. μSR spectroscopy of ordered magnets 105
3.4. Double relaxation 110
3.5. Data analysis 111
3.6. Determination of the muon site 114
3.7. Modeling of the internal field 116
3.8. Muon diffusion and magnetism (site averaging) 121
4. Elemental metals 122
4.1. Anisotropic spin fluctuations 124
4.2. Gadolinium 126
4.2.1. Paramagnetic region and critical behavior 127
4.2.2. Ferromagnetic region 129
4.2.3. High-pressure measurements 131
4.3. Holmium, dysprosium and erbium 132
4.3.1. Ambient pressure 132
4.3.1.1. Holmium 132
4.3.1.2. Dysprosium 134
4.3.1.3. Erbium 136
4.3.2. High-pressure measurements 138
5. Intermetallics 140
5.1. Singlet ground state systems 140

* This work has been supported by the BMBF, Federal Republic of Germany under contract 03-KA4-TU1-9, by US DOD grants F-49620-97-0297 (*AFOSR*) and -0532 (*BMDO*), and by the Swedish National Research Council.

5.1.1. Crystalline electric field (CEF) effects 140
5.1.2. μSR in singlet ground state systems 145
5.1.2.1. Praseodymium metal 146
5.1.2.2. $PrNi_5$ 147
5.1.2.3. $PrIn_3$ 148
5.1.2.4. $PrCu_2$ 149
5.1.2.5. PrP_x 149
5.1.2.6. $PrRu_2Si_2$ 150
5.1.2.7. $HoBa_2Cu_3O_7$ 150
5.1.3. Muon-induced effects 151
5.2. Simple cubic compounds 152
5.2.1. NaCl structure 154
5.2.1.1. UAs 156
5.2.1.2. UN 160
5.2.1.3. UP 160
5.2.1.4. USb 160
5.2.1.5. μSR response in AFM simple cubic compounds 162
5.2.1.6. CeAs 162
5.2.1.7. CeSb 166
5.2.1.8. DySb 167
5.2.1.9. Uranium monochalcogenides 167
5.2.2. CsCl structure 170
5.2.2.1. $LaAg_{1-x}In_x$ 171
5.2.2.2. CeAg and $CeAg_{0.97}In_{0.03}$ 171
5.2.2.3. DyAg 172
5.2.3. $AuCu_3$ structure 175
5.3. Laves-phase compounds 178
5.3.1. MAl_2 179
5.3.1.1. RAl_2 179
5.3.1.2. $AnAl_2$ (An=U, Np) 185
5.3.2. MT_2 (T = Fe, Co, Ni) 189
5.3.2.1. RT_2 189
5.3.2.2. AnT_2 191
5.3.3. MMn_2 and related compounds 193
5.3.3.1. YMn_2 193
5.3.3.2. Y(Tb)Mn_2 196
5.3.3.3. Y(Sc)Mn_2 197
5.3.3.4. Y(Mn,Al)$_2$ 199
5.3.3.5. Y(Mn,Fe)$_2$ 199
5.3.3.6. Y(Al,Fe)$_2$ 200
5.3.3.7. YMn_2 summary 201
5.3.3.8. RMn_2 with R=Gd, Tb, Dy 201
5.3.3.9. YCo_2 206
5.3.3.10. UMn_2 207
5.3.4. Other Laves phases 208
5.4. Binary compounds and alloys (other than Laves phases) 208
5.4.1. MX_2 compounds 208
5.4.1.1. $PrCu_2$ 208
5.4.1.2. $NdCu_2$ 208
5.4.1.3. R dihydrides and dideuterides 208
5.4.2. MX_3 compounds 209
5.4.2.1. $EuAs_3$ 209
5.4.2.2. UPd_3 209
5.4.3. MX_5 compounds 210
5.4.3.1. $GdNi_5$ 210
5.4.3.2. $TbNi_5$ 213
5.4.3.3. $DyNi_5$ 213
5.4.3.4. $ErNi_5$ 213
5.4.3.5. $TmNi_5$ 214
5.4.3.6. $YbNi_5$ 215
5.4.4. RGa_6 compounds 215
5.4.4.1. $CeGa_6$ 215
5.4.4.2. $NdGa_6$ 216
5.4.4.3. $GdGa_6$ 216
5.4.4.4. $TbGa_6$ 216
5.5. Ternary compounds 218
5.5.1. MTX 218
5.5.1.1. CeCuSn 218
5.5.1.2. UNiGa 219
5.5.1.3. UNiAl 220
5.5.1.4. Other UTX compounds 221
5.5.2. MT_2X_2 222
5.5.2.1. Y and La intermetallics 222
5.5.2.2. $CeRh_2Si_2$ 222
5.5.2.3. $PrCo_2Si_2$ 224
5.5.2.4. $PrRu_2Si_2$ 227
5.5.2.5. $NdRh_2Si_2$ 228
5.5.2.6. UT_2Si_2 with T=Co, Rh, Pt 228
5.5.2.7. $U(Pd_{1-x}Fe_x)_2Ge_2$ 229
5.6. Other compounds 231
5.6.1. $Gd_{0.696}Y_{0.304}$ 231
5.6.2. CeSi, CeGe 232
5.6.3. R_2In 232
5.6.4. $Y_6(Mn_{1-x}Fe_x)_{23}$ 233
5.6.5. YMn_{12} 233
5.6.6. $CeAgSb_2$ 234
5.6.7. $RFe_{9.5}Mo_{2.5}$ 234
5.6.8. RFe_6Al_6 235
5.6.9. RFe_4Al_8 236
5.6.10. RTC_2 237
5.7. Summary: μSR studies in R and An intermetallics 237
6. Non-metallic compounds 238

6.1. Binary oxides and halides 239
6.1.1. EuO 239
6.1.2. UO_2 and NpO_2 240
6.1.3. Rare-earth halides 243
6.2. Orthoferrites and other perovskites 243
6.3. Compounds showing giant magnetoresistance 245
6.4. Hard magnetic materials 248
7. Superconductors 250
7.1. Non-cuprate f-electron superconductors 251
7.2. Lanthanide magnetism in cuprates 255
7.2.1. The "214" phases 257
7.2.2. The "123" phases 259
7.2.2.1. R=Gd 261
7.2.2.2. R=Tb, Dy 262
7.2.2.3. R=Ho 262
7.2.2.4. R=Er 263
7.2.2.5. R=Pr 264
7.2.2.6. R=Nd 264
7.2.2.7. Other studies 265
7.2.3. The "2212" phase 265
7.2.4. Ruthenate hybrids 266
8. Disordered magnetism 267
8.1. Dilute spin glasses 269
8.2. More-concentrated magnetic disorder 270
8.2.1. Varying-power exponential relaxation 271
8.2.2. Kagomé dynamic relaxation 273
8.2.3. Static relaxation for non-Gaussian and non-Lorentzian field distributions 273
8.2.4. Inhomogeneous freezing 276
8.3. Results on disordered f-magnetism 277
8.3.1. Amorphous DyAg 277
8.3.2. Highly frustrated rare-earth systems 279
8.3.3. Rare-earth quasicrystals 281
8.3.4. Novel reduced-dimensionality systems 283
9. Correlated electron intermetallics 284
9.1. Overview 284
9.2. Kondo metals, semimetals and insulators 293
9.2.1. CeTSn (T=3d transition element) 293
9.2.1.1. CeNiSn 295
9.2.1.2. CePtSn and CePdSn 301
9.2.2. Pseudo-ternary compounds of type CeTSn 304
9.2.2.1. $La_xCe_{1-x}NiSn$ 304
9.2.2.2. $U_xCe_{1-x}NiSn$ 304
9.2.2.3. $CePt_xNi_{1-x}Sn$ 305
9.2.2.4. $CeCu_xNi_{1-x}Sn$ 306
9.2.3. CeRhSb and $La_xCe_{1-x}RhSb$ 312
9.2.4. The Kondo insulator YbB_{12} 314
9.2.5. Other Kondo metals 316
9.2.5.1. CePdSb 316
9.2.5.2. YbNiSn 318
9.2.5.3. $Yb(Cu_{1-x}Ni_x)_2Si_2$ 318
9.2.5.4. UCu_2Sn 319
9.3. Heavy-fermion compounds 319
9.3.1. Ce intermetallics 319
9.3.1.1. $CeRu_2$ 319
9.3.1.2. $CeAl_3$ 321
9.3.1.3. $CePb_3$ 323
9.3.1.4. $CeCu_5$, $CeCu_{5-x}Al_x$, $CeCu_{5-x}Ga_x$ 323
9.3.1.5. CeB_6 326
9.3.1.6. $CeCu_6$ 328
9.3.1.7. $CeRuSi_2$ 329
9.3.1.8. $CeCu_2Si_2$ and related compounds 331
9.3.1.9. $CeCu_2Ge_2$ 334
9.3.1.10. $CeRu_2Si_2$, $Ce_{1-x}La_xRu_2Si_2$, $Ce(Ru_{1-x}Rh_x)_2Si_2$ 335
9.3.1.11. $CeRu_2Ge_2$, $Ce(Ru_{1-x}Fe_x)_2Ge_2$ 340
9.3.1.12. CeT_2Sn_2 (T=Cu, Pd, Pt) 342
9.3.1.13. $CePd_2Al_3$ 347
9.3.1.14. $CeRh_3B_2$ 348
9.3.1.15. $Ce_3Au_3Sb_4$ 350
9.3.1.16. $Ce_3Pd_{20}Si_6$ and $Ce_3Pd_{20}Ge_6$ 351
9.3.2. U intermetallics 352
9.3.2.1. UGe_2 352
9.3.2.2. UPt_3, $U_{1-x}Th_xPt_3$, $U(Pd_xPt_{1-x})_3$ 352
9.3.2.3. UCu_5 361
9.3.2.4. UCd_{11} 364
9.3.2.5. UBe_{13}, $U_{1-x}Th_xBe_{13}$, $U_{1-x}Th_xBe_{13-y}B_y$ 364
9.3.2.6. U_2Zn_{17} 367
9.3.2.7. $U_{14}Au_{51}$ 370
9.3.2.8. URu_2Si_2, URh_2Si_2 and related compounds 370
9.3.2.9. URh_2Ge_2 375
9.3.2.10. UNi_2Al_3 and UPd_2Al_3 376
9.3.2.11. UNi_4B 381
9.3.3. Other heavy-fermion compounds 382
9.3.3.1. $PrInAg_2$ 382
9.3.3.2. Sm_3Se_4 (and Sm_2Se_3) 383
9.3.3.3. Sm_3Te_4 385

9.3.3.4. Yb_4As_3 385
9.3.3.5. YbBiPt and $Y_{0.5}Yb_{0.5}BiPt$ 386
9.3.3.6. YbPdSb 388
9.3.3.7. $YbAuCu_4$ 390
9.3.3.8. Yb_2Cu_9 392
9.3.4. Conclusions: heavy fermions 392
9.4. Non-Fermi-liquid behavior 393
9.4.1. General considerations 393
9.4.2. Non-Fermi-liquid materials 394
9.4.2.1. $CeCu_{6-x}Au_x$ 394
9.4.2.2. $UCu_{5-x}Pd_x$ 398
9.4.2.3. $Y_{1-x}U_xPd_3$ 400
9.4.2.4. $Ce(Cu_{1-x}Ni_x)_2Ge_2$ 402
9.4.2.5. $CeCoGe_{3-x}Si_x$ 403
9.4.2.6. Ce_7Ni_3 403
9.4.2.7. $CePt_2Si_2$ 406
9.4.2.8. U_2Pt_2In 407
9.4.3. Summary: NFL compounds 407
9.5. Intermediate valence 408
9.5.1. $CeSn_3$ (and $LaSn_3$), $CePd_3$ 408
9.5.2. $Ce_{1-x}Th_x$ 409
9.5.3. EuPdAs (and NdPdAs) 410
9.5.4. $Sm_{0.9}La_{0.1}S$ 412
10. Conclusions 412
Acknowledgements 414
References 414

List of symbols[1]

$A(t)$	observed forward–backward asymmetry (of decay positron count rate)
a	half width at half maximum of Lorentzian field distribution
a_0	initial asymmetry (of decay positron emission)
$\boldsymbol{B}$	magnetic field
$\boldsymbol{B}_{app}$	externally applied field in general
$\boldsymbol{B}_{con}$	contact field
$\boldsymbol{B}_{dem}$	demagnetizing field
$\boldsymbol{B}_{dip}$	dipolar field
$\boldsymbol{B}'_{dip}$	dipolar field inside Lorentz sphere
B_i	cartesian component of local field
$\boldsymbol{B}_{int}$	field at the muon site from internal sources
B_L	longitudinally applied field
$\boldsymbol{B}_{lor}$	Lorentz field
B_{rms}	root mean square field of a (Gaussian) field distribution
$\boldsymbol{B}_{sat}$	field required to achieve saturation magnetization
B_T	transverse applied field
$\boldsymbol{B}_\mu$	total magnetic field at muon site (local field)
$\langle B_\mu^2 \rangle$	second moment of local field distribution
C	specific heat
$C(E)$	energy distribution function of emitted positrons
c	speed of light
ce	conduction electrons
E	energy (in general)
E_f	Fermi energy
e	elementary charge
$G_x(t)$	transverse field (envelope) muon spin relaxation function
$G_z(t)$	zero field or longitudinal field muon spin relaxation function
$\mathcal{H}$	interaction Hamiltonian
$\hbar$	Planck constant
I	nuclear spin
$\boldsymbol{J}$	total electronic angular momentum
J	exchange integral
K	(muon) Knight shift constant
$\boldsymbol{k}$	(neutron) wave vector
k	Boltzmann constant
M_{dom}	domain magnetization
M_S	sample magnetization
m	mass
m_e	electron mass
m_p	proton mass
m_μ	muon mass
m_π	pion mass
$\mathcal{N}$	demagnetization factor

[1] Vectors are given in ***boldface italic*** type.

N	counts
N_B	backward counts
N_{bk}	background counts
N_F	forward counts
n	neutron
$n^\uparrow, n^\downarrow$	up (down) spin density
P	pressure
$P(B)$	probability of field magnitude $\|\boldsymbol{B}\|$; the magnetic field magnitude distribution
$P(T_K)$	distribution of Kondo temperatures
p	proton
p	exponent in stretched exponential muon spin relaxation
p_μ	muon momentum
p_ν	neutrino momentum
q	wave vector
$S(q, \omega)$	(neutron) scattering function
S_{th}	theoretical μSR signal function
S_μ	muon spin
T	absolute temperature
T_1	spin–lattice relaxation time
T_2	spin–spin relaxation time
T_C	Curie temperature
T_c	critical temperature (e.g., superconductors)
T_g	glass transition temperature
T_K	(single ion) Kondo temperature
T^*	Kondo lattice temperature
T_M	magnetic transition temperature in general
T_N	Néel temperature
T_Q	Quadrupolar ordering temperature
T_{RKKY}	Strength of RKKY interaction expressed as temperature
V	volume
$W(\theta)$	angular distribution of decay positrons
Z	nuclear charge
α	ratio of backward/forward counter efficiency
β	ratio of backward/forward initial asymmetry
γ	Sommerfeld constant of electronic specific heat
γ_p	proton gyromagnetic ratio
γ_μ	muon gyromagnetic ratio
Δ	Gaussian width of field distribution
Λ	general muon spin relaxation rate
λ	muon spin relaxation rate (exponential decay)
μ, (μ^+, μ^-)	muon (positive, negative)
$\vec{\mu}$	magnetic dipole moment
μ_B	Bohr magneton
μ_e	electron magnetic moment
μ_N	nuclear magneton
μ_p	proton magnetic moment
ν, ν_μ, ν_e	neutrino, muon neutrino, electron neutrino
ν_μ	muon spin precession frequency
$\bar{\nu}$	antineutrino
π, (π^+, π^-)	pion (positive, negative)
σ	muon spin relaxation rate (Gaussian decay)
$\vec{\sigma}_{ce}$	spin of conduction electron
σ_{VV}	Van Vleck width (of field distribution)
τ_c	correlation time in relaxation processes
τ_s	(magnetic) spin fluctuation time
τ_μ	muon lifetime
τ_π	pion lifetime
χ	magnetic susceptibility
ω_μ	muon spin precession angular frequency

List of acronyms

AFM	antiferromagnetism or antiferromagnetic or antiferromagnet
An	actinide (or actinoid)
APW	augmented plane wave (approximation)
bcc	body-centered cubic (crystal structure)
BCS	Bardeen–Cooper–Schrieffer
BOOM	Japanese pulsed muon facility at KEK
CEF	crystalline electric field
CERN	European Center for Nuclear Research, Geneva (Switzerland)